Materials Advances

ROYAL SOCIETY OF CHEMISTRY

PAPER

View Article Online
View Journal | View Issue

Cite this: *Mater. Adv.*, 2025, **6**, 8167

Polysulfone–chitosan hybrids *via* imine chemistry: a versatile strategy for functional bioactive materials

Oana Dumbrava,* Daniela Ailincai, Alexandru Anisiei, Irina Rosca, Daniela Rusu, Andrei Dascalu, Iuliana Stoica, Anca Filimon and Luminita Marin *

The paper aimed to develop a new approach to improve the hydrophilicity and bioactivity of polysulfone-based materials through covalent bonding with chitosan *via* imine or amine linkages. To achieve this, different synthetic strategies were employed, including the chloromethylation and etherification of polysulfone to introduce formyl functionalities along the polymer backbone. These formyl groups subsequently participated in condensation reactions with the amino groups of the chitosan chains, either on the surface or within the bulk. Additionally, reductive amination was applied to convert imine bonds into more stable amine linkages. A comprehensive characterization by ATR-FTIR, WXRD, UV-Vis, TGA, and SEM analyses confirmed the successful formation of the targeted hybrid materials, with a semicrystalline structure favoured by deep polymer blending through covalent bonding, high thermal stability and a porous morphology. Water uptake, contact angle and permeability assessments, conducted using dynamic vapor sorption and cup test methods, revealed significantly enhanced hydrophilicity, with water absorption levels reaching up to 45% and moderate wettability, with a water contact angle in the 60–90° range, swelling capacities of up to 2 g g^{-1}, and enzymatic degradation in lysozyme solutions reaching 45% mass loss over 21 days, depending on the chitosan content. Moreover, antioxidant activity evaluated *via* DPPH assays demonstrated a free radical scavenging capacity of approximately 20%, while antibacterial tests indicated the ability to inhibit bacterial growth by more than 30%, placing these materials in the bacteriostatic range. Overall, these findings support the modification of polysulfone with chitosan *via* imine bonds as an effective strategy for the design of advanced biomaterials and filtration technologies.

Received 17th June 2025,
Accepted 30th September 2025

DOI: 10.1039/d5ma00648a

rsc.li/materials-advances

1. Introduction

Membrane technology has experienced a great expansion in recent decades, being used in a multitude of fields such as chemical recovery, medical applications, wastewater recovery and water treatment.[1–5] The most commonly involved separation technology is ultrafiltration, the main features of which are simplicity, cost-effectiveness, low energy consumption, minimal or no chemical use, moderate operating temperatures and high-quality treatment results.[6,7] The membranes used in this process must exhibit hydrophilicity and a porous structure, as well as chemical stability in the presence of the feed solution.[8] Polysulfone (PSF) and polysulfone-based materials are extensively used as separation membranes due to their outstanding properties such as chemical and thermal stability, mechanical strength, as well as film-forming capacity.[1–5] Moreover, they are resistant to various sterilization methods,[9] which is why they are used in the biomedical field such as haemodialysis membranes.[10,11] However, their hydrophobic nature promotes the adsorption of humic substances, proteins and polysaccharides on the membrane surface, affecting the membrane permeability, efficiency and feasibility of the separation process, as well as its biocompatibility.[12,13] In order to overcome these considerable limitations and to enhance the hydrophilicity and antifouling properties, researchers have investigated various polysulfone structure modification techniques, such as bulk functionalization of the polymer structure, blending polysulfone with hydrophilic polymers, oligomers[14–16] and nanoparticles,[17,18] as well as grafting[19,20] or coating[21] on the surface of the polysulfone-based materials.[7] Among these chemical or physical modification techniques, the bulk one is more complex than the ones at the surface of the material, but it is slightly more efficient. Instead, the grafting method is simpler and leads to more stable structures compared to coating and blending methods, allowing the covalent binding of the hydrophilic agent to the

Petru Poni Institute of Macromolecular Chemistry, Iasi, Romania.
E-mail: dumbrava.oana@icmpp.ro, lmarin@icmpp.ro

membrane surface. In addition, this method does not completely modify the structure of the material, the hydrophilic agent being present only at the surface.[22] Among the hydrophilic agents used in order to enhance the affinity of the polysulfone-based membranes for water, the ones of natural origin are most preferred due to their sustainability, low cost, abundance and environmental friendliness. Chitosan, a biopolymer obtained by alkaline treatment of chitin, has received significant attention in the scientific community, due to its outstanding properties such as hydrophilicity, biocompatibility and biodegradability, as well as film forming properties.[9] The presence of hydroxyl and amine groups in the structure of chitosan endows the membrane with a positive charge and hydrophilicity, having a positive effect on permeability and solute removal.[23] Based on these considerations, there are a plethora of studies that have reported the modification of polysulfone membranes with chitosan, *via* blending and coating methods.[24–29] However, to the best of our knowledge, no covalent bonding of polysulfone with chitosan has been reported to date. Covalent bonding would offer the advantage of achieving a more homogeneous integration of the two components, leading to a consistent distribution of their functional properties and improved long-term stability. Unlike physical blends, which are prone to phase separation, covalently linked systems maintain structural and functional uniformity over time.

In this light, the work hypothesis of the study was to design a procedure to covalently bond chitosan and polysulfone into a new material with enhanced properties, such as thermal stability, porous morphology, capacity to transport water vapours and antioxidant activity. To fulfil this objective, the polysulfone has been functionalized with aldehyde units by etherification reaction with a phenolic aldehyde and further reacted with chitosan by imination followed by amination reactions, at the surface or in bulk. The obtained materials were structurally, supramolecularly and morphologically characterized by FTIR, NMR and UV-vis spectroscopy, X-ray diffraction, thermal gravimetric analysis, differential scanning calorimetry, scanning electron microscopy and atomic force microscopy. Furthermore, relevant properties such as hydrophilicity, water permeability, degradation in wet media, and antimicrobial and antioxidant activities were investigated, in order to assess their propensity to be applied in applications which require moisture management, infection control and mitigating oxidative stress, such as haemodialysis membranes, but also transdermal drug release systems, wound dressings, or biosensors.

2. Materials and methods

2.1. Materials

Chitosan (147 kDa, DD = 82% determined by viscosimetry and NMR (Fig. S1 and S2)), acetic acid (99.89%), tin(IV) chloride (98%), chlorotrimethylsilane (98%), paraformaldehyde (95%), *N*,*N*-dimethylformamide (DMF), sodium carbonate (99.5%), and sodium borohydride (98%) were purchased from Sigma Aldrich Co. St. Louis, MO, USA and used as received. Polysulfone (35 kDa, polydispersity index = 2.18) has been purchased from Sigma Aldrich Co., St. Louis, MO, USA, and purified by reprecipitation from chloroform in methanol. Chloroform and methanol were purchased from Chemical Company and distilled with the aid of a rotary evaporator, while the ethanol was purchased from ChimReactiv and was dried on molecular sieves (3 Å, Fluka) before use. 4-Hydroxybenzaldehyde (98%) (4-HBA) was purchased from Fluka and used without further purification.

2.2. Synthesis of polysulfone – chitosan materials

In order to covalently react polysulfone with chitosan, several synthetic pathways (Scheme 1) were followed: (1) chloromethylation of polysulfone, (2) etherification of chloromethylated polysulfone, (3) grafting of chitosan on the surface of materials based on formylated polysulfone or (4) grafting of formylated polysulfone on the surface of materials based on chitosan *via* imine linkages, as well as (5) bulk synthesis of formylated polysulfone-*graft*-chitosan and (6) reductive amination reaction of (3), (4) and (5) compounds. The synthetic pathways are represented in Scheme 1 and detailed procedures are described below.

2.2.1. Synthesis of chloromethylated polysulfone. The introduction of the chloromethyl group on the polysulfone backbone was accomplished following a synthetic procedure similar to that previously reported in the literature.[30] In a three-neck flask, equipped with a magnetic stirrer and a reflux condenser, 6 g (0.013 mol of repeating units) of polysulfone were dissolved in 240 mL of chloroform at 50 °C. After the complete solubilization, 6.12 g (0.2 mol) of paraformaldehyde, 0.2 mL (0.003 mol) of tin (IV) chloride and 25 mL (0.2 mol) of chlorotrimethylsilane were added and maintained under stirring (650 min^{-1}) for 72 hours. Then, the chloromethylated polysulfone was isolated from the reaction mixture through the precipitation in methanol, washed 3 times with 300 mL water in order to remove the $SnCl_4$, filtered through a G4 funnel and dried under vacuum at 40 °C overnight. ^{1}H-NMR (400.13 MHz, $CDCl_3$, δ, ppm): 7.88–7.85 (H-3C, H-3D), 7.37 (H-3′B), 7.26–7.24 (H-3A, overlapped with deuterated solvent residual peak), 7.18–7.16 (H-3B), 7.04–7.00 (H-2C, H-2D), 6.95–6.94 (H-2A), 6.85–6.83 (H-2B), 4.54 (–CH_2–Cl), 1.71 (–C(CH_3)$_2$, overlapped with residual water from deuterated solvent); ^{13}C NMR (100.6 MHz, $CDCl_3$, δ, ppm): 162.05–161.56 (C-4C, C-4D), 152.96–152.84 (C-1A), 151.12–151.00 (C-1B), 147.78–147.36 (C-4A), 147.19–146.77 (C-4B), 135.93–135.26 (C-4C, C-4D), 129.84–129.74 (C-3C, C-3D), 129.47 (C-3′B), 129.12–128.99 (C-3B), 128.46 (C-3A), 120.15–120.10 (C-2B), 119.90–119.83 (C-2A), 117.83–117.70 (C-2C, C-2D), 42.51 (–*C*(CH$_3$)$_2$), 40.99 (*C*H$_2$–Cl), 30.98–30.92 (–C(*C*H$_3$)$_2$). Yield: 98%.

2.2.2. Synthesis of formylated polysulfone (FPSF). The formylated polysulfone was synthesized by chemical modification of the chloromethylated polysulfone *via* the Williamson etherification reaction with 4-hydroxybenzaldehyde (4-HBA). 6 g (0.012 mol) of chloromethylated polysulfone was dissolved in 144 mL DMF to obtain a 4.1% solution. Separately, 1.53 g of 4-HBA (0.012 mol, taking account of the 85% purity of the aldehyde) and 1.62 g of Na_2CO_3 (0.015 mol) were added to 60 mL DMF (5.2% solids in solvent) to obtain a fine suspension

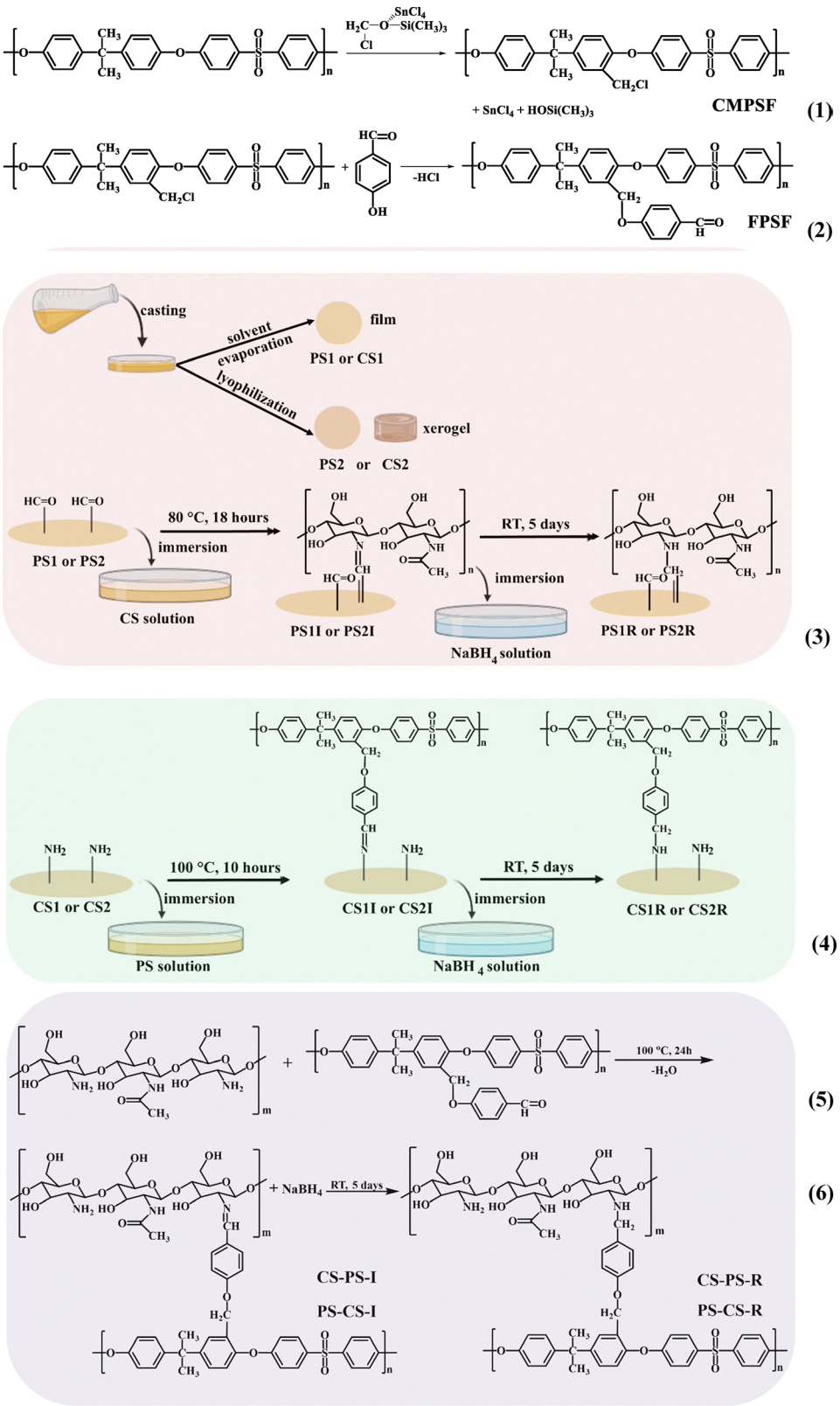

Scheme 1 The main synthetic steps followed in this study: chloromethylation of polysulfone (1); etherification of chloromethylated polysulfone (2); grafting of chitosan on the surface of materials based on formylated polysulfone or grafting of formylated polysulfone on the surface of materials based on chitosan *via* imine or amine units ((3) and (4)) and bulk synthesis of formylated polysulfone-*graft*-chitosan *via* imine or amine units ((5) and (6)).

which was stirred for 10 minutes at room temperature. After that, the suspension was added dropwise to the chloromethylated polysulfone solution and the reaction mixture was stirred and heated at 100 °C for one hour. Formylated polysulfone was isolated from the reaction mixture in the same manner as the chloromethylation derivative. ^{1}H-NMR (400.13 MHz, $CDCl_3$, δ, ppm): 9.82–9.81 (–C*H*O), 7.85–7.83 (H-3C, H-3D), 7.72–7.67 (H-3E), 7.40 (H-3′B), 7.26–7.21 (H-3B, H-3A, overlapped with deuterated solvent residual peak), 7.01–6.97 (H-2C, H-2D), 6.95–6.91 (H-2A, H-2B), 6.85–6.80 (H-2E), 5.06–5.04 (–CH_2), 1.69 (–C(CH_3)$_2$, overlapped with residual water from deuterated solvent); ^{13}C NMR (100.6 MHz, $CDCl_3$, δ, ppm): 190.6 (CHO), 163.15 (C-1E), 161.88–161.70 (C-1C, C-1D), 152.76–152.69 (C-1A), 150.57 (C-1B), 147.77–146.70 (C-4A, C-4B), 135.65–135.25 (C-4C, C-4D), 131.76 (C-3E), 130.04 (C-4E), 129.63–129.60 (C-3C, C-3D), 128.83 (C-3′B), 128.53–128.36 (C-3A, C-3B), 127.46–127.39 (C-2′B), 120.30–119.73 (C-2A, C-2B), 117.57–117.30 (C-2C, C-2D), 114.81 (C-2E), 65.43 (–CH_2) 42.53–42.32 (–C(CH_3)$_2$), 30.85–30.80 (–C(CH_3)$_2$). Yield = 97%. To facilitate name tracking of the obtained materials, films and xerogels containing formylated polysulfone in their structure will contain the PS code in the sample name (*e.g.* **PS1** – films based on formylated polysulfone and **PS2** – xerogels based on formylated polysulfone).

2.2.3. Grafting of chitosan on the surface of the formylated polysulfone-based materials. The grafting of chitosan on the surface of the formylated polysulfone-based materials through imine bonds was done following the next procedure: formylated polysulfone films or xerogels, previously obtained by pouring a 2% solution of formylated polysulfone in DMF (500 mg of formylated polysulfone in 25 mL DMF) and evaporating the solvent, or, respectively, lyophilization, were immersed in a 1% chitosan solution 0.7% acetic acid (350 μL glacial acetic acid in 50 mL water). The reaction took place at 80 °C for 18 hours and the mass ratio between formylated polysulfone and chitosan was 1 : 1. After completion of the synthesis, the materials were removed and washed with ethanol prior to being dried over molecular sieves.

2.2.4. Grafting of formylated polysulfone on the surface of the chitosan-based materials. The grafting of formylated polysulfone on the surface of chitosan-based materials through imine bonds was carried out by the following experimental procedure: 500 mg of chitosan was dissolved in 0.7% solution of acetic acid (175 μL glacial acetic acid in 25 mL water) and after its complete dissolution, the solution was poured into a Petri dish and dried by slow evaporation of the solvent or by lyophilization. Subsequently, the film, respectively, the chitosan xerogel, was immersed in a 50 mL of 1% formylated polysulfone solution in DMF. The mass ratio between the two polymers was equal. The reaction proceeded for 10 hours at 100 °C. At the end of the synthesis, the materials were taken off and washed with anhydrous DMF to remove the unreacted formylated polysulfone.

2.2.5. Bulk synthesis of polysulfone-imine-chitosan materials. The bulk synthesis of formylated polysulfone-*graft*-chitosan was achieved *via* the following steps: 100 mg of chitosan was dissolved in 0.7% aqueous solution of acetic acid (70 μL acetic acid in 10 mL water) and after its complete dissolution, 10 mL DMF was added dropwise to the chitosan solution under high magnetic stirring. In parallel, 100 mg of formylated polysulfone was dissolved in 13.2 mL DMF. After 3 hours of magnetic stirring, the chitosan solution was added dropwise to the formylated polysulfone solution to obtain an opalescent mixture which was stirred vigorously (1000 rpm) at 100 °C, for 24 hours. During the synthesis, the colour of the reaction mixture turned from white to yellow, a signature of imine bond formation. At the end of the synthesis, the reaction mixture was poured into a Petri dish and within 48 hours the two solvents were evaporated, thus obtaining the film called **CS-PS-I**. In a similar manner was obtained the film called **PS-CS-I**, with the difference that the formylated polysulfone solution was added dropwise to the chitosan solution.

2.2.6. Reductive amination of the polysulfone-imine-chitosan materials. The reduction of imine linkage between chitosan and polysulfone was achieved by immersing the materials in a solution of $NaBH_4$ in ethanol with a concentration of 0.4% (0.48 g $NaBH_4$ in 120 mL ethanol), at room temperature. Since the reaction remained incomplete after 48 hours, it was allowed to proceed over the weekend, achieving complete conversion after five days, as confirmed by FTIR spectra. Afterwards, the materials were isolated from the $NaBH_4$ solution and washed several times with 300 mL ethanol and dried in an oven under vacuum to provide the final material with a yield of 98%.

2.3. Characterization methods

The NMR spectra of polysulfone, chloromethylated polysulfone and formylated polysulfone were recorded with a Bruker Avance NEO 400 MHz spectrometer (Bruker, Ettlingen, Germany). The investigated polymers were solubilized in deuterated chloroform ($CDCl_3$) or deuterated dimethyl sulfoxide (DMSO-d_6) for analysis, and the NMR assignments of the signals corresponding to hydrogen and carbon atoms were done based on bidimensional spectra (H, H COSY; H, C-HMBC; H, C-HSQC). Atom numbering for NMR assignments is shown in the following scheme (Scheme 2):

Based on ^{1}H-NMR spectra, the degree of substitution (DS) of the chloromethylated polysulfone was calculated with eqn (1) and that of the formylated polysulfone with eqn (2):

$$\mathrm{DS} = \frac{I_{\mathrm{CH_2Cl}}}{I_{\mathrm{3C,3D}}} \times 2 \quad (1)$$

where $I_{\mathrm{CH_2Cl}}$ is the integral value corresponding to the peak located at 4.54 ppm corresponding to the two protons of –CH_2Cl, and $I_{\mathrm{3C,3D}}$ is the integral value of the multiplet located at 7.88–7.85, corresponding to the 4 protons from the C and D aromatic rings, adjacent to the sulfone group, which is not affected by any overlapping with the signal of other protons.

$$\mathrm{DS} = \frac{I_{\mathrm{CH_2-O-}}}{I_{\mathrm{CHO}}} \times 2 \quad (2)$$

where $I_{\mathrm{CH_2-O-}}$ is the integral value for the two protons of the etheric bridge (5.06–5.04 ppm) and I_{CHO} is the integral value for the proton of the aldehyde group (9.82–9.81 ppm).

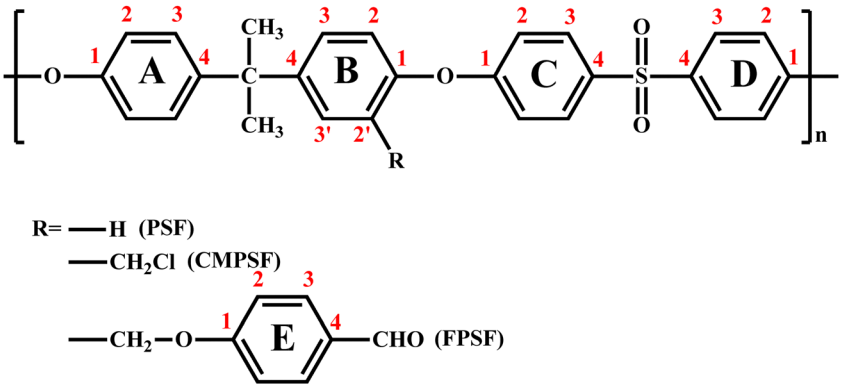

Scheme 2 Atoms numbering for NMR assignments.

Xerogels based on polysulfone or chitosan were obtained by a freeze-drying process, using a LABCONCO Free Zone Freeze Dry System equipment, at −54 °C and 1.510 mbar, for 24 h.

Fourier-transform infrared (FTIR) spectra of the pristine polysulfone and functionalized polysulfones, as well as of the films and xerogels based on formylated polysulfone and chitosan were registered with a Bruker spectrophotometer (VERTEX 70), from 4000 to 600 cm^{-1}, by the ATR method. The obtained spectra were processed with OPUS 6.5 software.

UV-Vis spectra of materials based on polysulfone and chitosan were recorded in the solid state, using an Agilent Cary 60 UV-Vis spectrophotometer (Agilent Technologies, Inc. Headquarters, Santa Clara, CA, USA).

The thermal stability of the studied samples was investigated over a temperature range from 30 °C to 600 °C, using a Discovery TGA 5500 thermogravimetric analyzer (TA Instruments) with a probe holder of 100 μL platinum pan at a heating rate of 10 °C min^{-1}.

Differential scanning calorimetric (DSC) measurements of several representative samples were carried out by using a TA instrument DSC 250, under nitrogen purge. The device was temperature and sensitivity calibrated with indium, according to standard procedures. The samples, weighing approximately 2.5 mg each, were loaded in punched and sealed aluminium crucibles and DSC curves were recorded on a heating–cooling–heating scan, at a heating/cooling rate of 10 °C min^{-1}.

Wide angle X-ray diffraction was performed using a Benchtop Miniflex 600 Rigaku diffractometer (Tokyo, Japan) with CuKα-emission. The diffractograms were registered at room temperature, from 2 to 50° (2θ), with a scanning step of 0.06° and a recording speed of 4° min^{-1}.

The morphology of the investigated materials was analysed using a scanning electron microscope SEM EDAX—Quanta 200 (Eindhoven, Germany) equipped with an Energy Dispersive X-ray (EDX) module, at an accelerated electron energy of 10 keV. The elements' percent was measured at three different points and the average value was considered.

The topography of the materials was investigated by atomic force microscopy (AFM) using an NTEGRA system provided by NT-MDT Spectrum Instruments Company from Zelenograd, Moscow, Russia. The surface aspect of the samples was studied under atmospheric conditions at 21 °C using an NSG 03 cantilever (TipsNano OÜ, Tallinn, Estonia) with a resonance frequency of 67 kHz and a force constant of 0.25 N m^{-1}. The cantilever having a length of 150 ± 10 μm, a width of 24 ± 7 μm, a thickness of 1.75 ± 0.75 μm, and a tip curvature radius of 10 nm was working in tapping mode. For AFM image acquisition and processing, Nova 1.1.1.19891 and 1.0.26.1443 software (NT-MDT Spectrum Instruments, Zelenograd, Moscow, Russia) employed a scanning frequency of 0.8 Hz and scan lengths of 20, 10, and 5 μm.

Static contact angle measurements were conducted using a KSV CAM-101 goniometer, equipped with a Hamilton syringe and a CDD camera connected to a PC. A drop of 1 μL water, ethylene glycol or diiodomethane was placed on the surface of polysulfone and/or chitosan based materials and the contact angle values were recorded immediately. The measurements were carried out three times for each test liquid and the average values were reported.

The swelling behaviour of the materials was analysed in phosphate buffer saline solution (PBS), pH = 7.4, following the next experimental procedure: pieces of films or xerogels, with an area of 0.5 cm^2 (1.9 ± 1 mg), were placed in Petri dishes, over which 5 mL of PBS was added. The samples were weighed, from time to time (0.25, 0.5, 1, 2, 3, 24 and 48 hours), in order to determine the swelling degree, by applying the following equation:

$$SD = \frac{(W_t - W_0)}{W_0} \quad (3)$$

where SD = swelling degree, W_t = the weight of the sample at a certain moment and W_0 = the initial weight of the sample.

The dynamic water vapor sorption (DVS) capacity of the samples was measured on a fully automated gravimetric analyzer IGAsorp supplied by Hiden Analytical, at 25 °C, in the 0–90% relative humidity (RH) range.[31] The average pore size (eqn (4)) was calculated as a function of the maximum water uptake (W) (eqn (5)):

$$\text{average pore size} = \frac{2 \times W}{100 \times \rho \times A} \quad (4)$$

where ρ is the adsorbate phase density; A is the Brunauer–Emmett–Teller (BET) surface area;

$$W = \frac{W_w - W_d}{W_d} \times 100 \quad (5)$$

where W_d is the weight of the dried sample and W_w is the weight of the sample at a certain moment of determination.

Water vapor transmission rate (WVTR) was monitored following the cup method (ASTM E96–05) protocol.[32] The bottle was filled with ultrapure water, weighed and sealed with film or xerogel samples with an area of 0.07065 cm^2 and a thickness value between 62 and 121 μm (in the case of films and xerogels of polysulfone modified at the surface with chitosan or chitosan films iminated or aminated at the surface, as well as in the case of the films obtained *via* bulk condensation between these two polymers) and between 967 and 1517 μm (in the case of chitosan xerogels, pristine or modified at the surface), and placed in an oven at 37 °C. During 14 days, the bottles were weighed after different periods of time (1, 2, 3, 9, 10, 11, and 14 days) and the WVTR was calculated with the following equation:

$$\mathrm{WVTR} = \frac{\Delta_m}{\Delta_t} \times A \quad (6)$$

where Δ_m is the mass of water loss after a certain period of time (g), Δ_t is the time interval (days), and A is the effective transfer area.

The *in vitro* enzymatic degradation of materials was investigated by monitoring the mass loss of the films and xerogels after immersing and maintaining them for 7, 14 and 21 days in a lysozyme solution (376 U mL^{-1}) prepared in PBS 7.4. In order to compare, one sample was also immersed in a PBS solution of pH 7.4, without adding lysozyme. Pieces of films and xerogels with a dry mass of 5 ± 0.3 mg each were added in a volume of lysozyme solution to reach 1 mg mL^{-1} and incubated at 37 °C for a certain period of time (7, 14 and 21 days). Every 3 days, the lysozyme solution was replaced with a fresh one, in order to avoid the enzyme inactivation. At the end of the exposure time to the enzymatic degradation, the samples were taken from the lysozyme solution, washed with double distilled water to remove the salts, lyophilized and weighed in order to calculate the mass loss, by using the following equation:

$$W_{loss} = \frac{W_0 - W_t}{W_0} \times 100 \quad (7)$$

where W_{loss} is the weight loss of the sample, W_0 represents the initial weight of the sample and W_t is the weight of the sample after a certain period of time of incubation in the lysozyme solution.

The radical scavenging activity of the materials based on chitosan and polysulfone was investigated by the DPPH method, in solid state, following an experimental protocol reported in the literature.[33] Pieces of films or xerogels, weighing 10 mg each, were immersed in 2.857 mL of an ethanolic solution of DPPH with a concentration of 62.5 μM. After 1 hour of incubation, at 37 °C, in the dark, the UV-Vis absorbance was recorded at 517 nm and the radical scavenging activity (RSA) for each sample was calculated by using the following equation:

$$\mathrm{RSA} = \frac{A_{DPPH} - A_s}{A_{DPPH}} \times 100 \quad (8)$$

where A_{DPPH} is the absorbance of the DPPH solution and A_s is the absorption of the DPPH solution after one hour of exposure to each sample.

The antibacterial activity of the samples' surfaces was investigated *via* a modified Japanese industrial standard JIS Z2801: 2000[34] against two different reference strains *Staphylococcus aureus* ATCC25923 (*S. aureus*) and *Escherichia coli* ATCC25922 (*E. coli*). The bacterial strains were refreshed in nutrient broth (NB) for 24 h at 37 °C. The samples were cut into pieces of 10 mm and were placed in sterile Petri dishes. Then, 100 μL of the inoculum (0.5 McFarland) was instilled on the sample's surface and left to incubate for 24 hours at 37 °C. Subsequently, the samples were rinsed repeatedly and the resulting suspension was transferred into 96-well plates. The bacteriostatic activity and efficacy of samples after incubation with the microorganisms were assessed by MTS assay using the CellTiter 96® AQueous One Solution Cell Proliferation Assay (Promega, Madison, WI, USA), according to the manufacturer's instructions. After 23 hours, the samples were removed from the plates and the MTS reagent was added for 1 hour. After the formazan formation, the absorbance reading was performed at 490 nm on a FLUOstar® Omega microplate reader (BMG LABTECH, Ortenberg, Germany). Experiments were done in triplicate, and the treated cell viability was expressed as a percentage of the control cells' viability. Graphical data were expressed as means ± standard error of the mean.

All experiments were done in triplicate, and the results were expressed as the arithmetic mean ± the standard deviation of the mean values for each sample, and they were statistically processed using GraphPad Prism 9, using either One-Way ANOVA Tukey's multiple comparison *post hoc* test or Two-Way ANOVA Tukey's multiple comparison *post hoc* test.

3. Results and discussion

3.1. Synthesis and structural characterization of materials based on polysulfone and chitosan

A series of materials based on polysulfone and chitosan covalently bonded through imine or amine units was prepared by applying different synthetic routes (Scheme 1). An important role in achieving this goal consisted of the chemical modification of the polysulfone through (1) chloromethylation and (2) Williamson etherification of the chloromethylated polysulfone with a phenolic aldehyde to obtain polysulfone functionalized with formyl units, able to react with amine units of chitosan to give covalent imine bonds, which further could be transformed into amine bonds by reduction reaction.

The successful functionalization of polysulfone with chloromethyl and subsequently with formyl groups was confirmed by ^{1}H-NMR, ^{13}C-NMR and IR spectroscopy. ^{1}H-NMR spectrum of chloromethylated polysulfone (CMPSF) displayed the

characteristic signals of $-CH_2-Cl$ (4.54 ppm) as well as the change in the number, position and integral value of the signals characteristic of the aromatic protons of the ring B, in line with the chemical environment change induced by the chlorine, while ^{13}C-NMR showed all the corresponding carbon atoms (Fig. 1 and Fig. S3–S5 and explanation in the SI, considering the importance of this derivative in the synthesis of the formylated polysulfone, the spectra were recorded in different solvents for a correct evaluation of the multiplicity and integral ratio).[35] Based on the ^{1}H-NMR spectrum, the degree of substitution of CMPSF was found to be 0.9 chloromethyl groups per monomeric unit. After Willimson's reaction of CMPSF with 4-HBA, the ^{1}H-NMR spectrum changed, reflecting the successful functionalization with formyl units. Thus, in the ^{1}H-NMR spectrum of **FPSF** was observed the occurrence of a new signal at 9.82-9.81 ppm, characteristic for the formyl proton and also signals at 7.72–7.67 (H-3E) and 6.85–6.80 (H-2E) ppm characteristic of the aromatic protons of the aromatic ring of 4-HBA (Fig. 1 and Fig. S3).[36] Moreover, following the substitution of the chlorine atom with the 4-HBA residue, the signal corresponding to the two protons of the methylene group shifted to 5.06–5.04 ppm. This shift is attributed to the higher electronegativity of the oxygen atom relative to chlorine, coupled with the mesomeric electron-withdrawing effect of the formyl group, both of which result in increased deshielding of the respective protons. As a result, the protons in $-CH_2-O$ resonate at a higher frequency, corresponding to a higher chemical shift of 5.06–5.04 ppm. Furthermore, minor changes in the position of the aromatic protons' signals were also noticed, in line with the modification of the chemical environment that induces alterations in the electronic conjugation and symmetry of the aromatic rings.[37] The absence of the $-CH_2-Cl$ signal at 4.54 ppm in the formylated polysulfone spectrum highlights the total conversion of the CMPSF into the formylated polysulfone, also confirmed by the similar substitution degree: 0.9 benzaldehyde groups per monomeric unit. Besides, the successful of formylation has been proved by the presence of all the signals characteristic of the carbon atoms in the ^{13}C-NMR spectrum, with the clear occurrence of the formyl carbon at 190.6 ppm (Fig. S3).

A complementary method which was used to highlight the introduction of formyl moieties on the polysulfone backbone was FTIR spectroscopy. A comparative analysis of the FTIR spectra of the pristine polysulfone and the functionalized ones (Fig. 2) revealed the presence of new absorption bands in the case of **FPSF**, at 1690 and 1596 cm^{-1}, characteristic of the vibration of C=O group and the C=C bonds from the aromatic ring of the benzaldehyde moiety.[38] Moreover, the presence of the absorption bands at 1033 and 1245 cm^{-1} (superimposed with the one at 1250 cm^{-1}, specific to the vibration of the aryl

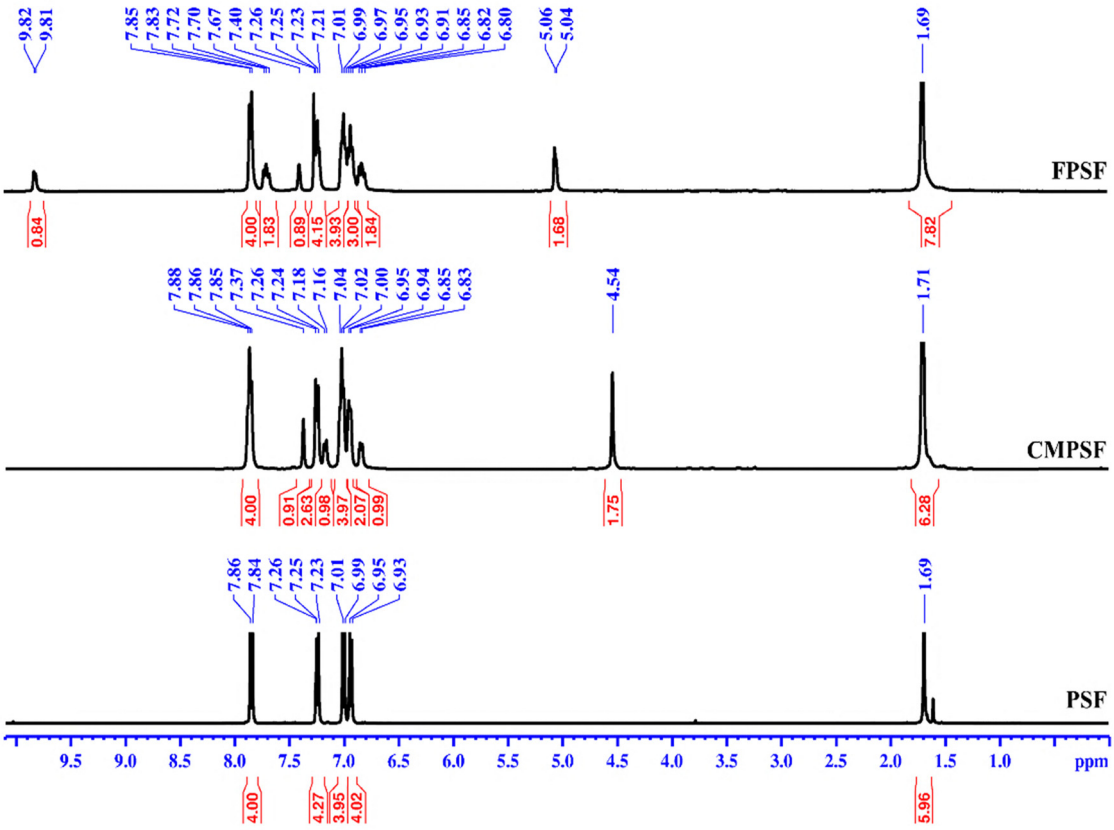

Fig. 1 ^{1}H-NMR spectra of polysulfone, chloromethylated polysulfone and formylated polysulfone (spectra with magnified domains are shown in Fig. S3 in the SI).

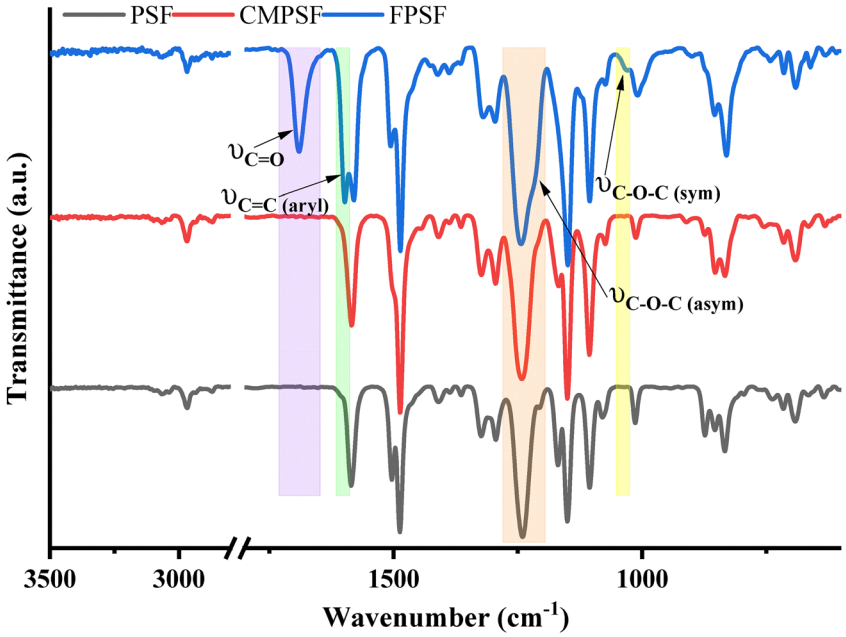

Fig. 2 FTIR spectra of polysulfone, chloromethylated polysulfone and formylated polysulfone.

ether group), which correspond to the vibration of aliphatic and aromatic ether vibration, indicates the presence of the ether bridge between the methyl group attached to the polysulfone backbone and the benzaldehyde fragment.[39] Other bands, such as the asymmetric and symmetric vibration of the SO_2 group at 1319, 1294 and 1150 cm^{-1} and the stretching of aliphatic and aromatic C–H bonds around 2968 and 3064 cm^{-1} can also be observed in the spectra.[40]

The results of the NMR and FTIR spectroscopic analyses highlighted the successful synthesis of polysulfone bearing formyl moieties, which was used to react with chitosan by condensation reaction to give imine bonds, and their further reduction to give secondary amine units. In order to confirm this synthetic pathway, FTIR spectra were recorded for all investigated materials, both films and xerogels (Fig. 3). These showed relevant changes compared to those of the chitosan or **FPSF** precursors, confirming the formation of imine or secondary amine bonds between the two polymers. Thus, in all materials resulted from the imination of **FPSF** with chitosan, regardless of the method used for their obtaining, either by imination at the surface (**CS1I**, **PS1I**, **CS2I**, and **PS2I**) or by bulk synthesis (**CS-PS-I** and **PS-CS-I**), it was observed that the broad band specific to the C–N amide bond vibration of the acetylated glucosamine units of chitosan (1642 cm^{-1}) was replaced by a sharp band with an absorption maximum at 1650 cm^{-1}, attributable to the characteristic imine units overlapped with amide bands.[41,42] Another aspect that suggests the success of the imination reaction between the two polymers is the disappearance or decrease in intensity of the absorption band at 1690 cm^{-1}, specific to the vibration of the aldehyde group in the **FPSF** structure, thus demonstrating its total or partial conversion into imine units. Moreover, the diminishing of the chitosan amine group vibration band (1551 cm^{-1}) highlights their consumption of during the condensation reaction.

In the FTIR spectra of aminated materials, prepared either by surface modification (**CS1R**, **PS1R**, **CS2R**, **PS2R**) or by bulk synthesis (**CS-PS-R** and **PS-CS-R**), it can be observed that the characteristic vibrational band of the imine groups decreased in intensity or disappeared, suggesting their partial or total conversion into secondary amines upon treatment with $NaBH_4$. In addition, in the FTIR spectra of the tested films or xerogels, the presence of absorption bands representative of chitosan and formylated polysulfone was also noted, indicating the lack of degradation products. Thus, in the fingerprint domain, the bands corresponding to the vibration of the C=C bonds of the aromatic rings of the formylated polysulfone can be observed at 1484 and 1572 cm^{-1} (superimposed in some cases with the band specific to the amine group), while the bands specific to the vibration of the aliphatic C–H bonds of chitosan, appeared at ~1409 and 1376 cm^{-1}. Moreover, the absorption band characteristic of the symmetrical stretching of the diphenyl ether units in the formylated polysulfone structure can be observed at 1244 cm^{-1}, while the specific bands of the C–O–C bond in the chitosan structure appear at 1150, 1070 and 1020 cm^{-1}. Other absorption bands that support the bonding of the two polymers are the vibration of the amine and hydroxyl groups in chitosan in the spectral range 3500–3000 cm^{-1},[41] as well as the symmetric and asymmetric stretching vibration of the sulfone group in the polysulfone macromolecular chain at 1152, 1295 and 1329 cm^{-1}.[43] Nevertheless, a potential reduction of the non-iminated formyl groups to alcohols cannot be assessed, due to the superposition with the absorption bands of the hydroxyl units in the chitosan structure.

To have a complementary confirmation of the successful imination and reductive amination reactions, the absorption

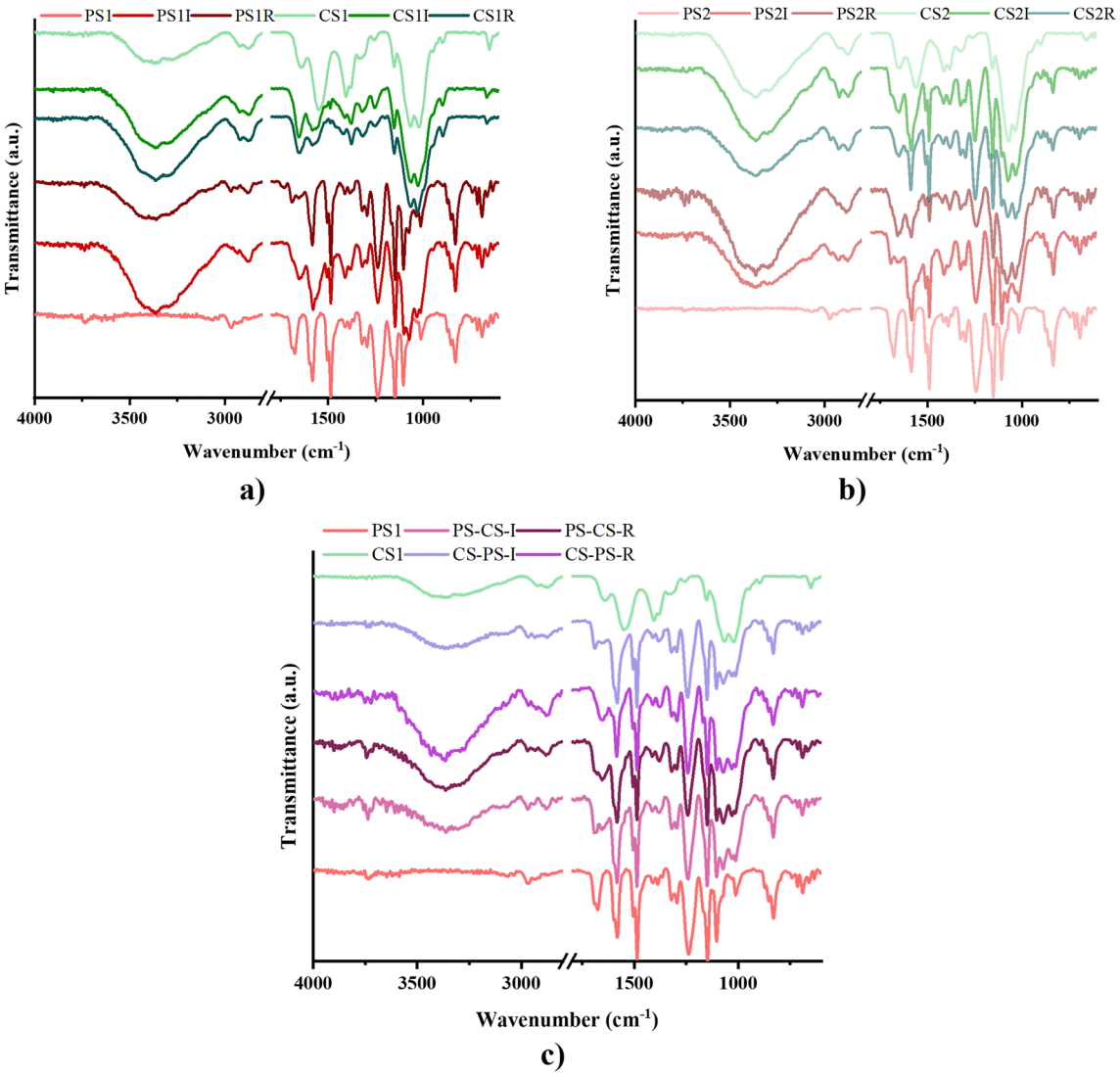

Fig. 3 FTIR spectra of (a) surface iminated or aminated formylated polysulfone (**PS1I**, **PS1R**) or chitosan (**CS1I**, **CS1R**) films and pristine polymeric films (**PS1**, **CS1**); (b) surface iminated or aminated xerogels based on chitosan (**CS2I**, **CS2R**) or formylated polysulfone (**PS2I**, **PS2R**) and pristine polymeric xerogels (**CS2**, **PS2**); (c) films prepared by the bulk reaction of formylated polysulfone and chitosan, *via* imine (**PS-CS-I**, **CS-PS-I**) or amine bonds (**PS-CS-R**, **CS-PS-R**).

spectra of the studied materials were also recorded and compared to those one of chitosan and formylated polysulfone, respectively. All the iminated materials presented in their spectra an absorption band around 330–340 nm, which corresponds to the π–π* transitions of the imine moiety, confirming once again its formation between chitosan and polysulfone chains (Fig. 4).[44,45] In the spectra of the aminated materials, absorption bands at lower wavelengths, 306–315 nm, can be observed, which correspond to the n–π* transitions of the secondary amine bond, strengthening the hypothesis that the reductive amination reaction of the imine bond proceeded successfully.[46]

Additional information regarding the successful surface or bulk bonding of chitosan and formylated polysulfone was given by the SEM-EDAX analysis recorded for the investigated materials (Fig. 5 and Fig. S6). Therefore, the comparative EDAX pattern reveals the occurrence of the signal characteristic for the sulphur atom of FSPF in the EDAX spectra of the **FPSF** modified chitosan (**CS1I**, **CS1R**, **CS2I**, **CS2R**, **CS-PS-I**, **CS-PS-R**, **PS-CS-I**, **PS-CS-R**), as well as the presence of the signal characteristic for the nitrogen atom of chitosan in the EDAX spectra of the chitosan modified **FPSF** (**PS1I**, **PS1R**, **PS2I**, **PS2R**, **CS-PS-I**, **CS-PS-R**, **PS-CS-I**, **PS-CS-R**).

3.2. Morphological and thermal investigation

To gain a deeper insight into the influence of surface and covalent bonding of chitosan and formylated polysulfone on the supramolecular organization of the studied materials, wide-angle X-ray diffraction (WAXD) patterns were recorded (Fig. 6). The pristine chitosan control materials exhibited broad, overlapping diffraction bands with two reflection maxima around 20° and 12°. The position and intensity of these reflections varied slightly depending on the manufacturing process

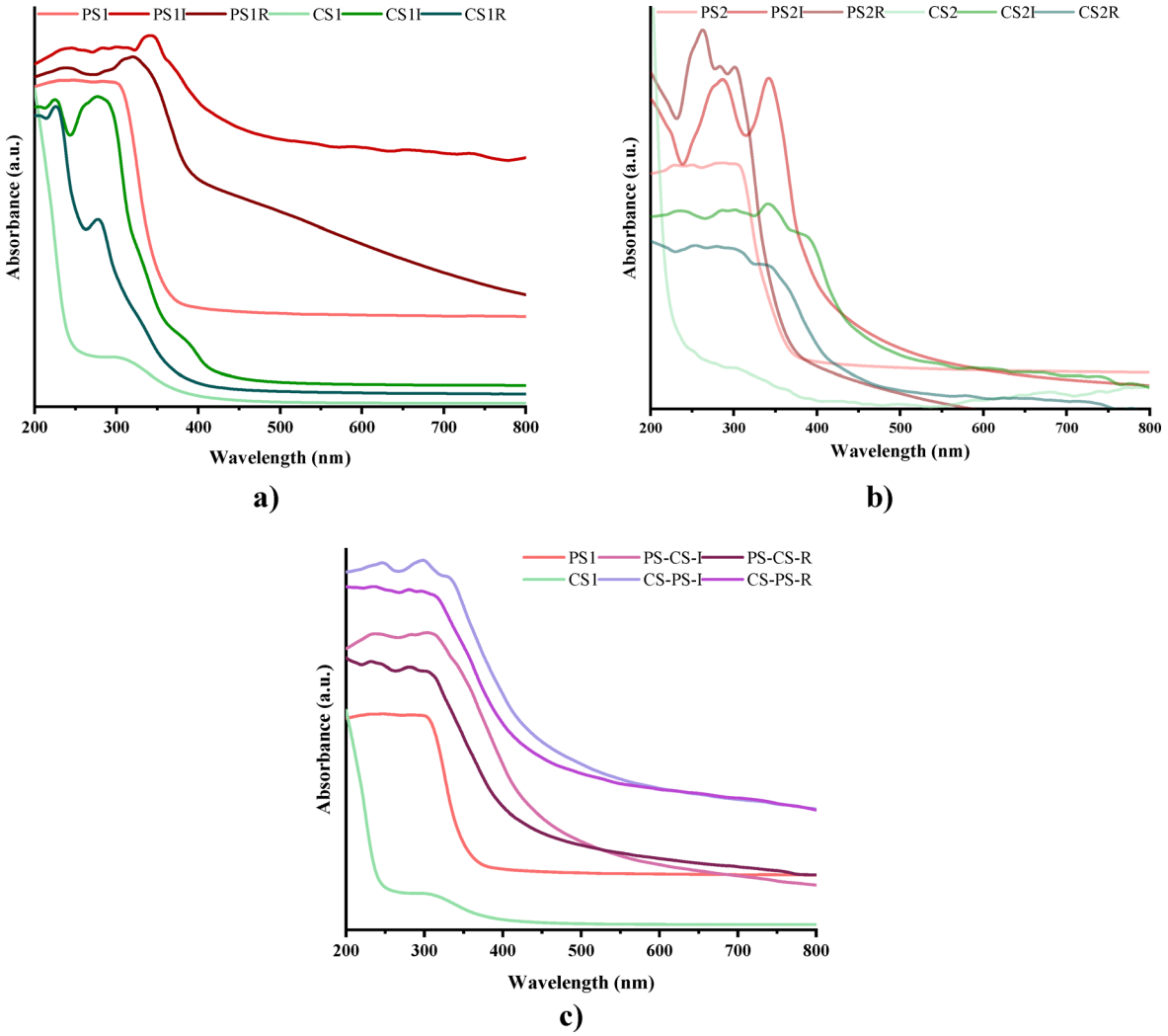

Fig. 4 UV-Vis spectra of (a) surface iminated or aminated films based on formylated polysulfone (**PS1I**, **PS1R**) or chitosan (**CS1I**, **CS1R**) and pristine polymeric films (**PS1**, **CS1**), (b) surface iminated or aminated xerogels based on chitosan (**CS2I**, **CS2R**) or formylated polysulfone (**PS2I**, **PS2R**) and pristine polymeric xerogels (**CS2**, **PS2**), (c) films prepared by bulk reaction of formylated polysulfone and chitosan, *via* imine (**PS-CS-I**, **CS-PS-I**) or amine bonds (**PS-CS-R**, **CS-PS-R**).

(*i.e.* casting *vs.* lyophilization). Their occurrence is well documented in literature and is a signature of chitosan's ability to self-organize through inter- and intra-molecular interactions during solvent removal, leading to the formation of crystalline domains dispersed within an amorphous matrix.[47,48]

The pristine formylated polysulfone materials (**PS1**, **PS2**) also displayed two broad diffraction bands with maxima around 18° and 5°, attributed to an amorphous morphology.[49] This is consistent with a low self-order capacity of the polysulfone chains, owing to their non-linear molecular structure characterized by bulky aromatic groups and sulfone linkages.[45] As in the case of chitosan, the diffraction patterns of **FPSF** materials exhibited slight variations depending on the processing method.

Regarding the diffraction patterns of the iminated and aminated materials, some certain changes were observed. The most significant ones occurred in the case of the materials synthesized *via* the bulk method, for which the mass ratio of the two polymers was 1 : 1. In these samples, the main diffraction maximum (around 20°) appeared at an intermediate position compared to the pristine polymers, suggesting a blending of the two components. This effect was likely facilitated by covalent imine bonding, which brings the polymer chains into close proximity. Furthermore, supporting this hypothesis, the **FPSF** diffraction peak at 5° shifted to lower angles and split into two distinct reflections of low intensity at 4.4° and 3°, corresponding to interlayer distances of 20 Å and 28 Å, respectively. This suggests the presence of a layered periodicity of short range, most likely taking the shape of small-sized clusters, potentially formed due to hydrophilic/hydrophobic segregation (Table S1).[48]

In contrast, these diffraction pattern modifications were less pronounced in materials modified *via* surface grafting, likely due to the unbalanced polymer ratio in these systems. However,

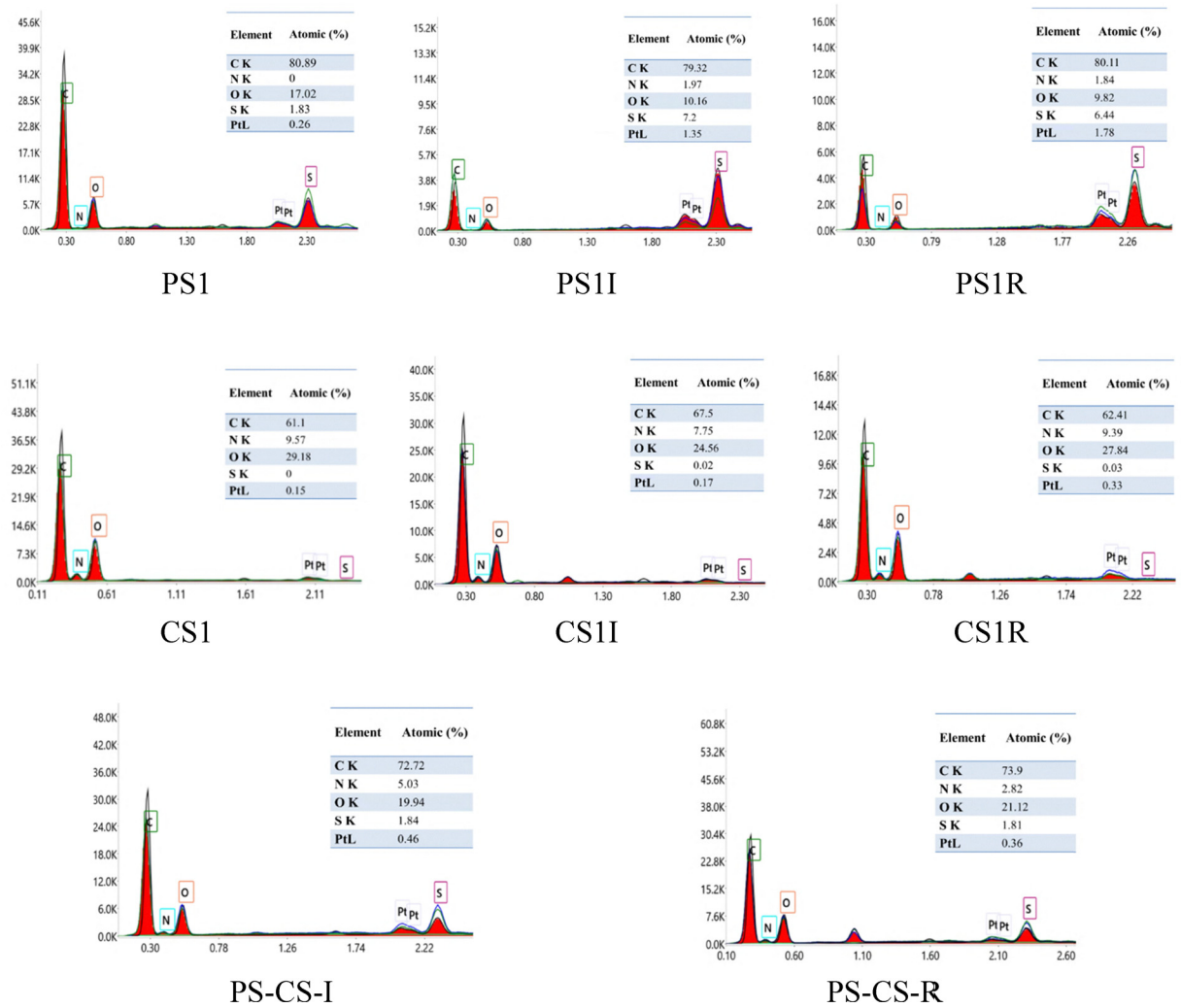

Fig. 5 Representative SEM-EDAX analysis of the investigated samples.

in chitosan modified with polysulfone, a noticeable shift in the reflection corresponding to intra- and inter-chain distances towards lower angles was observed, indicating an increase in intermolecular spacing. This phenomenon is easily explained considering the preparation method: during the surface grafting, the polysulfone solution in dimethylformamide (DMF) acted as a swelling agent for chitosan, facilitating polysulfone chain penetration and disrupting chitosan's native supramolecular organization.[50] In contrast, for polysulfone materials modified with chitosan at the surface, no significant structural modifications were detected, which is consistent with the lack of swelling effect of polysulfone in aqueous chitosan solutions used for surface grafting.

The *d*-spacing values were calculated using Bragg's law based on the measured diffraction angles from the XRD profiles of each sample and the results are presented in Table S1.

Thermogravimetric analysis of the investigated materials was assayed in order to evaluate the impact of the chemical modification on thermal stability. The TGA and DTG curves are presented in Fig. 7. The pristine chitosan and polysulfone polymers presented characteristic degradation steps: (i) a sharp degradation peak around 290 °C for chitosan and (ii) a broad degradation peak around 500 °C for polysulfone.[51,52] Both polymers presented slight mass losses up to 200 °C, attributed to the water loss in chitosan and ether bond cleavage in polysulfone.

The analysis of the degradation profile of the studied materials revealed useful information for understanding the forces governing their formation.

First, the samples prepared by bulk synthesis of the two polymers in a 1 : 1 mass ratio showed well-defined degradation steps for the two polymers, but their position was modified compared to the pristine polymers, in agreement with the disruption of their intermolecular forces by mixing. The general trend was the shift of the degradation maximum to lower temperatures, in agreement with the formation of chitosan-rich polysulfone and polysulfone-rich-chitosan domains, as suggested by X-ray diffraction. Exception to this trend, the degradation maximum of chitosan in the iminated samples shifted slightly to higher temperatures (Fig. 7e and f).

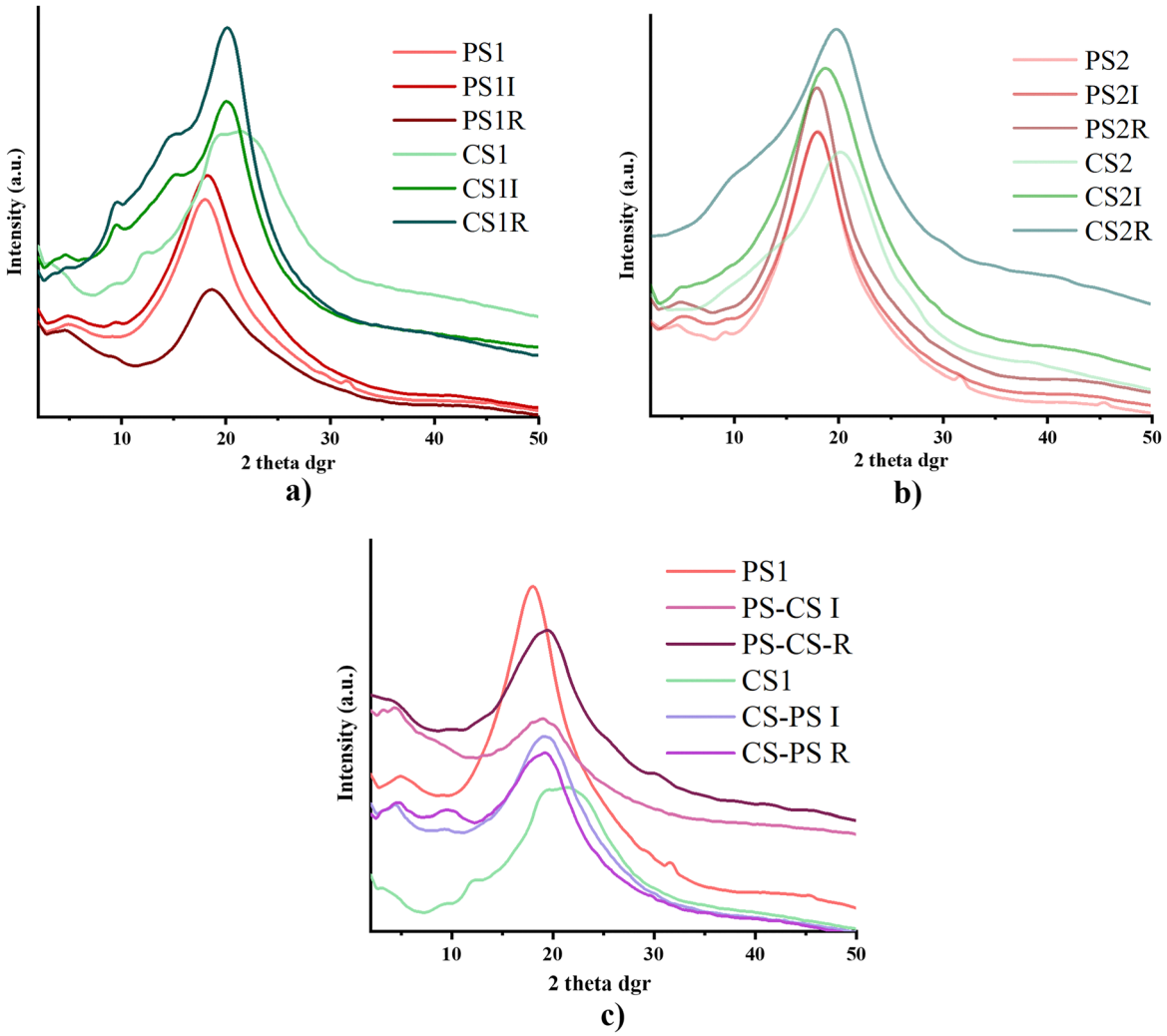

Fig. 6 XRD diffractograms of (a) surface iminated or aminated films based on polysulfone (**PS1I**, **PS1R**) or chitosan (**CS1I**, **CS1R**) and pristine polymeric films (**PS1**, **CS1**), (b) surface iminated or aminated xerogels based on polysulfone (**PS2I**, **PS2R**) or chitosan (**CS2I**, **CS2R**) and pristine polymeric xerogels (**PS2**, **CS2**), (c) films prepared by bulk reaction of formylated polysulfone and chitosan, *via* imine (**PS-CS-I**, **CS-PS-I**) or amine bonds (**PS-CS-R**, **CS-PS-R**).

A relatively similar behaviour was recorded for the samples obtained by surface modification of the xerogels, but with smaller changes in the degradation temperature, easily interpreted by the lower blending of the two polymers, less intimately mixed compared to bulk synthesis.

A completely different behaviour was recorded for the films modified at the surface. While the degradation step characteristic of chitosan followed a similar trend described for the other samples (in agreement with the polysulfone infiltration in the chitosan matrix suggested by X-ray), the degradation step characteristic to polysulfone encountered an antagonistic behaviour: it consistently shifted to higher temperatures indicating a strengthening of the polysulfone chain interactions when modified at the surface with chitosan (Fig. 7a and b). An explanation for this unusual behaviour may be the formation of an extremely thin layer of chitosan at the surface of polysulfone films, anchored by covalent bonding *via* imine or amine units, hindering the thermal motion of the polysulfone segments at the interface.[53]

Another observation is related to the intensity of mass loss associated with each degradation step. In the case of chitosan films reacted at the surface with **FPSF**, the degradation steps characteristic to **FPSF** are extremely low, indicating a very thin film of **FPSF** on the surface of chitosan films, likely anchored by imine units. Conversely, in the case of the polysulfone films modified with chitosan at the surface, the degradation step characteristic to chitosan was quite pronounced, indicating a higher amount of chitosan, probably due to the high potential of chitosan to self-aggregate, leading to thicker layers of semicrystalline chitosan. Its absence after the reduction reaction can be attributed to the removal of chemically unbound chitosan from the reaction medium.

Overall, the thermal degradation of the studied materials follows the degradation profile of the two polymers. This is confirmed by the percentage of ash residue, which showed variations from 24 to 53%, depending on the dominant polymer and also on the manufacturing process (Table S2). The increase in the ash residue percentage is easily attributed to the

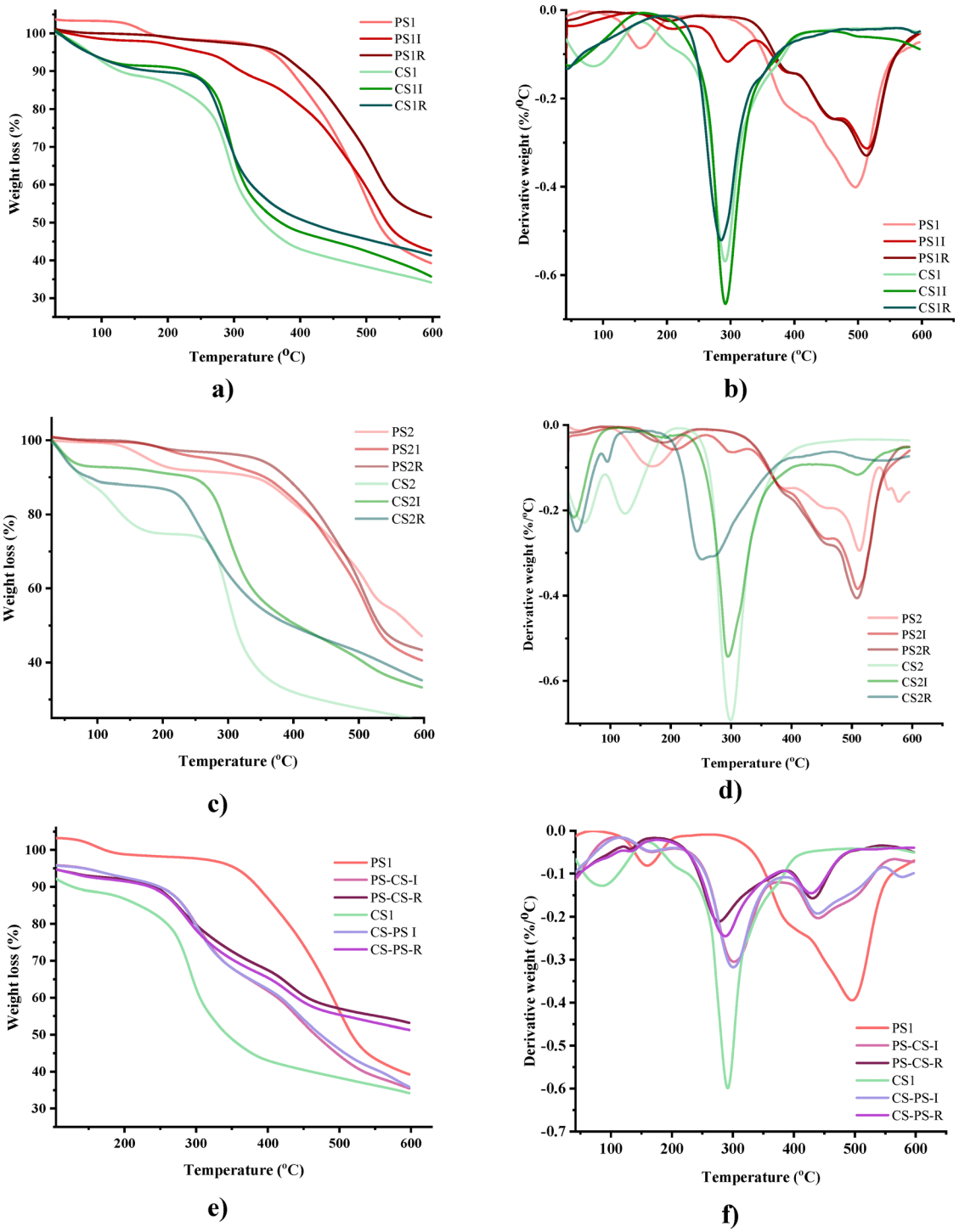

Fig. 7 TGA and DTG curves of (a) and (b) surface iminated or aminated polysulfone (**PS1I**, **PS1R**) or chitosan (**CS1I**, **CS1R**) films and pristine polymeric films (**CS1**, **PS1**), (c) and (d) surface iminated or aminated xerogels based on polysulfone (**PS2I**, **PS2R**) or chitosan (**CS2I**, **CS2R**) and pristine polymeric xerogels (**CS2**, **PS2**), (e) and (f) films prepared by bulk reaction of formylated polysulfone and chitosan, *via* imine (**PS-CS-I**, **CS-PS-I**) or amine bonds (**PS-CS-R**, **CS-PS-R**).

contribution of the more thermally stable aromatic **FPSF** in the case of chitosan films modified with **FPSF** at the surface. However, this explanation is not suitable in the case of **FPSF** films modified at the surface with chitosan, whose polysaccharide nature is more easily degradable. The rational explanation for this behaviour is the occurrence of strong interactions between the two polymers, strengthening the material, and consequently, its thermal resistance,[54] but also the presence in its structure of aromatic rings from the polysulfone chain, which through degradation are transformed into more thermally stable

carbonaceous residue, thus significantly increasing the residue mass.[55]

The hypothesis of the intimate mixing of the two polymers was confirmed by the DSC measurements which showed a more complex thermal behaviour compared to the pristine polymers, with a broad endotherm with many maxima in the first heating step, attributable to the polymer domains rich in the other polymer (Fig. S7).

The morphology of polysulfone and chitosan-based materials, obtained by imination or amination reactions, was investigated by scanning electron microscopy on the surface and cross-sections (Fig. 8) and atomic force microscopy (Fig. S8). The pristine polysulfone film exhibits a compact structure with irregular large pores, with high density at the surface. Following the grafting of chitosan onto the surface of polysulfone based materials, either in film or xerogel state, the internal structure of the materials, revealed by cross-section images, appeared to have a "spongy like" pattern, with small pores with a diameter of approximately 0.5 μm in the case of films and larger pores with a diameter between 0.86 and 7.78 μm in the case of xerogels.[56] This is a rather surprising result, suggesting that an increase in porosity occurs during the chemical modification. The only rational explanation may be that formyl units endow the polysulfone with a slight hydrophilicity, which allows the infiltration of water molecules during the chemical modification in the aqueous media of chitosan, leading to a porous morphology.

In the case of chitosan-based films, pristine or functionalized on the surface with polysulfone *via* imine or amine units, a parallel-lamellar structure can be observed, with intercalated voids within the polymeric layers.[57] On the other hand, chitosan xerogels, pristine as well as the ones modified with polysulfone, showed a porous morphology, with micrometric interconnected pores, whose sizes range between 30 and 60 μm.[58] Following the surface functionalization, the pore walls appeared thicker, in line with the grafting of the polysulfone on their surface.

The morphology of films prepared by bulk synthesis indicates a quite compact morphology with small microasperities, with a lower level of pore alignment compared to neat or surface-modified chitosan-based films.

A more detailed surface analysis using atomic force microscopy revealed a generally rough topography, with no consistent trend in average roughness values, likely reflecting the influence of the manufacturing process rather than the specific chemical composition (Fig. S8 and Table S3). However, it was observed that bulk synthesis resulted in materials with a significantly rougher surface compared to those modified at the surface, while modification of the xerogels produced *via* lyophilization led to a smoother surface.

3.3. Materials behaviour in wet media

In order to use a material in the biomedical field, it is crucial to investigate its structural stability and also its ability to facilitate/promote the transport of body fluids and bioactive substances when exposed to humidity.[59] Therefore, taking into consideration these requirements, the swelling behaviour of the understudied materials was monitored over 48 hours, in a media simulating the physiological environment (saline PBS, at 37 °C) (Fig. 9). In most cases, the samples have attained the equilibrium state in less than 1 hour with a swelling degree from 1.02 to 0.75 g g^{-1}, indicating a good ability to transport bioactive ingredients.[60] The exception to this situation was the pristine chitosan samples that showed a significant increase in the swelling degree in the first 30 minutes, followed by a progressive decrease (Fig. S9). Not surprisingly, this behaviour can be explained by a competition between swelling and solubilization/degradation of chitosan during the hydration process,[61–63] owing to its hydrophilic nature and high affinity for saline solutions,[64] and favoured by the presence of residual acetic acid within material's structure.[61,64,65]

As expected, by combining chitosan with polysulfone, the degree of swelling of films and xerogels decreased statistically significant compared to neat chitosan materials, by almost an order of magnitude (Fig. 9 and Fig. S9), in line with the creation of a hydrophobic layer on the surface, which partially prevents the interaction of the polar groups in the chitosan structure with the PBS. Higher values were recorded for the xerogel samples, in line with their more porous morphology, which facilitates the penetration of PBS solution and the interaction with the free hydrophilic groups in the material structure.

In the case of materials based on formylated polysulfone, no significant improvement in swelling behaviour was observed after surface modification with chitosan, despite its hydrophilicity. This may be a consequence of the strengthening of polysulfone materials by interfacial interactions with chitosan, as suggested by the TGA data. The imine derivatives showed slightly higher swelling rates compared to the aminated ones, a behaviour correlated with the role of hydrophilicity enhancers of these groups.[48]

The materials obtained through bulk synthesis exhibited swelling values slightly higher than those of polysulfone-based materials but significantly lower than those of pure chitosan. This confirms an intimate mixing of the two polymers, apparently with chitosan well confined into polysulfone. Overall, the swelling capacity was higher compared to neat polysulfone and other polysulfone/chitosan blend materials reported in literature, emphasizing the beneficial impact of covalent crosslinking through hydrophilic imine bonds.[8]

Given the critical role that a biomaterial's surface plays in its interactions with cells and biological fluids, affecting processes such as cell adhesion and protein adsorption, the surface characteristics were evaluated through contact angle measurements to assess wettability and surface energy (Fig. S10 and Table S4).[66–68] The contact angle values ranged from 30 to 120°, without a consistent trend, indicating that surface roughness likely exerts a more significant influence than surface chemistry in the case of these materials (Fig. S8).[69] Nevertheless, the observed contact angles fell within the 60–90° range for the majority of samples, corresponding to moderate wettability, a characteristic known to support cell adhesion and proliferation.[67] Additionally, the surface energy, calculated based on contact angle measurements using both polar and non-polar

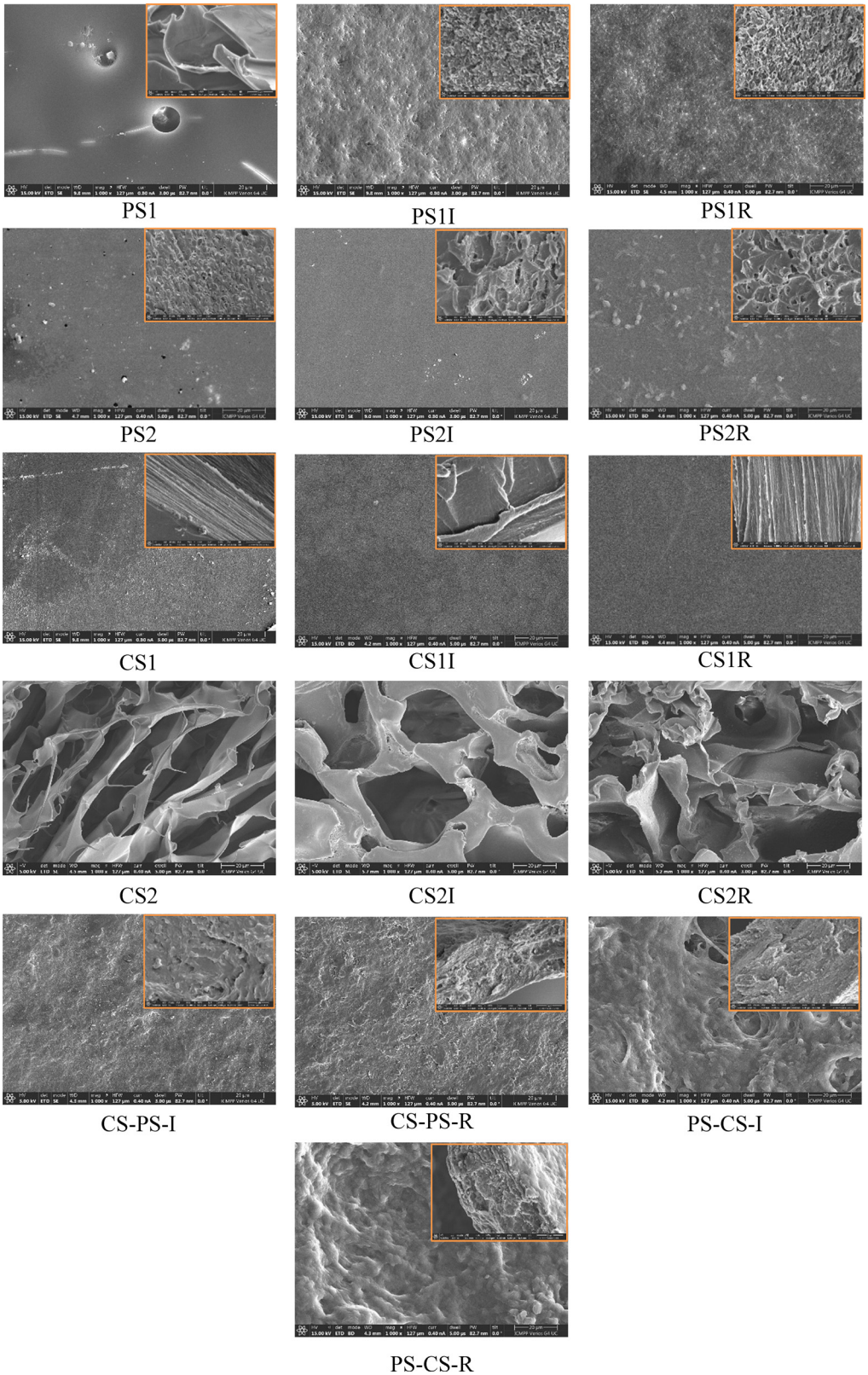

Fig. 8 SEM micrographs of the studied samples, captured from both the surface and cross-section (inset). Each image is labelled with the corresponding sample code.

solvents, indicated that surface or bulk modification with chitosan significantly increased the surface energy, placing it in the optimal range for promoting cell attachment and growth (Fig. S11 and Table S4).[70]

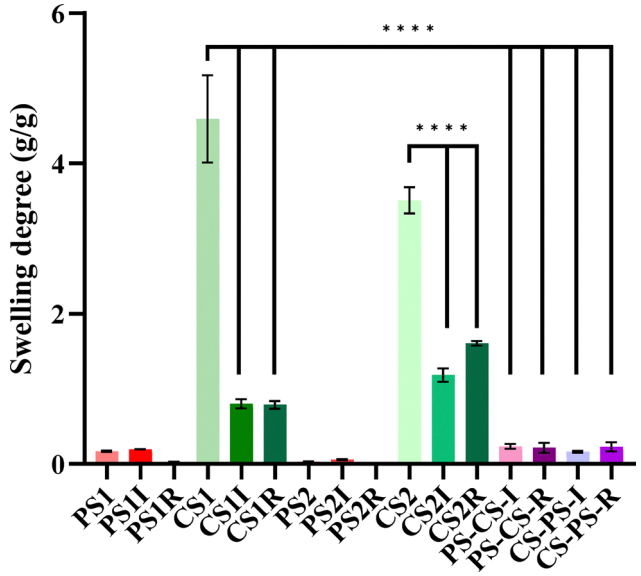

Fig. 9 Swelling degree of the investigated materials in PBS (pH = 7.4) after 48 hours (****$p < 0.0001$).

To gain a more precise understanding of the hydrophilicity of the studied materials and their ability to uptake liquids, their water sorption/desorption behaviour was investigated. This analysis provided insights into the migration of water through their structure, as well as on the factors influencing their absorption or release of water. The water vapor sorption–desorption isotherms recorded under dynamic conditions are presented in Fig. 10. According to the IUPAC classification, the adsorption isotherms of the unmodified formylated polysulfone (**PS1**, **PS2**) samples correspond to a reversible type III isotherm.[71] This type of isotherm is characteristic of hydrophobic surfaces, where adsorbate-adsorbate interactions dominate over the adsorbate-adsorbent ones. Consequently, adsorption occurs in multilayers without the formation of a complete monolayer on the surface.

However, upon modification with chitosan, the isotherm profile shifts to a type II isotherm, indicating an increased contribution of surface adsorption. This transition is more pronounced in xerogels and materials obtained *via* bulk synthesis, where the characteristic ''knee'' of the type II isotherm becomes more defined. This suggests an enhancement in surface-related adsorption, although the measured adsorption values remain relatively low and insufficient for a detailed surface area determination (Table S5).

Changes in the weight of materials were observed as a function of relative humidity (RH). Thus, at RH values higher than 20%, the weight change values increased exponentially. Therefore, the adsorption isotherms of the samples exhibit a H3-type hysteresis loop: as relative humidity increases, the adsorption and desorption curves become steeper, indicating a rapid increase in the adsorption volume. Even at high relative humidity values, the plateau phenomenon in water adsorption does not occur, suggesting the presence of wedge-shaped or groove-like pores within the material's structure. These findings align with SEM observations, which revealed a tendency for chitosan-based materials to form a lamellar morphology, while polysulfone-based materials exhibited an interconnected porous network.[72] It is expected that this morphology at the micro-level to be reproduced at the nano-level. For comparison purposes, the values of sorption capacity (% d.b.), specific surface area ($m^2\ g^{-1}$) and the amount of water retained in the monolayer ($g\ g^{-1}$) of the materials are presented in Table S3. From the sorption/desorption curves, it can be noted that the modification of the polysulfone films or xerogels with chitosan had an impact on an increase in water uptake from ~8 to ~20%, while the functionalization of chitosan with **FPSF** had an impact on a decrease from ~55 to ~38%, highlighting the role of chitosan in improving the liquid uptake (Fig. 10d–i and Fig. S12). Moreover, the bulk synthesis of the PS-CS materials led to water uptake values from 35 to 45%, suggesting that this method is suitable for controlling the material properties. This aspect can be correlated with the disruption of the hydrophilic–hydrophobic balance of the tested materials, considering that chitosan is rich in hydrophilic groups capable of binding the water molecules (–OH, –N=CH, $–NH_2$, and –NH–).

Water vapor transmission rate (WVTR). The rate at which water vapor penetrated the materials based on chitosan and/or formylated polysulfone was monitored for 14 days, at body temperature, 37 °C. After the first 24 hours, the materials presented high WVTR values, statistically significantly higher for those containing a high amount of chitosan compared to those based on polysulfone (Fig. S13). Over time, the water transport capacity of the materials decreased, in correlation with their swelling ability, decreasing the pore volume. However, these films and xerogels still presented very high permeability values, between 2311 and 12 628 $g\ m^{-2}$ per day, comparable to those of materials designed for food packaging.[73] However, compared to other polysulfone based materials and even chitosan-based materials, these values are very high,[74–77] most probably due to some microcracks formed during manipulation/experiment, favoured by their rigid nature. Nevertheless, the water transmission rate correlates well with the material's ability to adsorb/desorb water, as observed by DVS measurements. It is worth noting that higher WVTR values were recorded for the materials in which chitosan is the dominant polymer, followed by those in which chitosan is in equal mass ratio to polysulfone, and lastly, by those only covered with a thin chitosan layer. This behaviour can be explained by the presence of polar groups in the structure of chitosan-based materials that form hydrogen bonds with water molecules, thus facilitating their diffusion. The presence of imine bonds appeared to be also beneficial for water transfer, most probably due to their hydrophilicity and, possibly, due to their reversible character, which promotes the cleavage in the presence of water molecules, favouring their transfer.

A particular case was observed in the performance of formylated polysulfone films modified at the surface with chitosan, through imine or secondary amine units. Apparently, the surface modification with chitosan decreased the water vapor diffusion capacity, in line with the strengthening of polysulfone films through covalent bonding and interfacial forces with

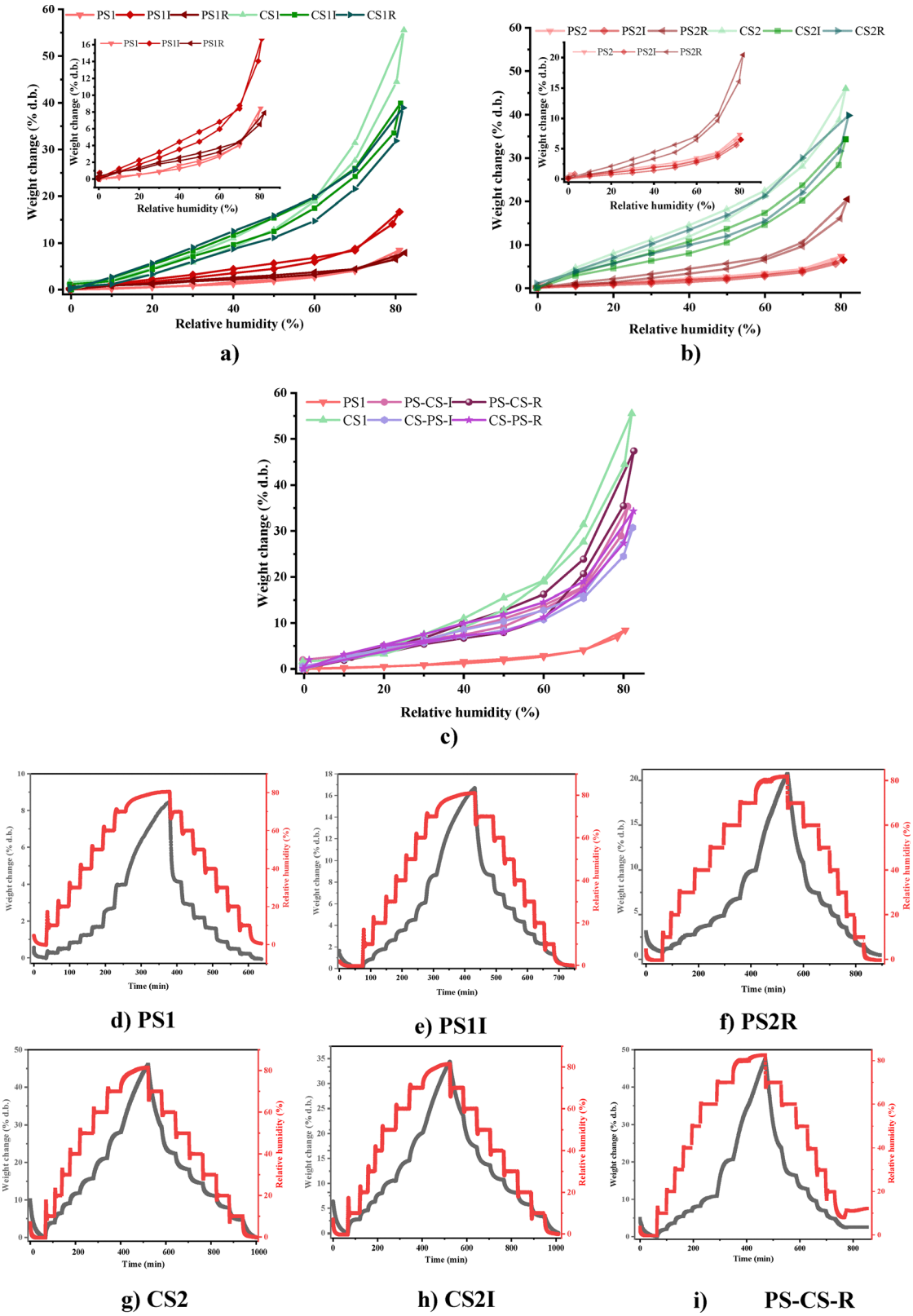

Fig. 10 Water vapor sorption isotherms of the understudied samples compared to reference materials: (a) surface iminated or aminated polysulfone (**PS1I**, **PS1R**) or chitosan (**CS1I**, **CS1R**) films and pristine polymeric films (**PS1**, **CS1**); (b) surface iminated or aminated xerogels based on polysulfone (**PS2I**, **PS2R**) or chitosan (**CS2I**, **CS2R**) and pristine polymeric xerogels (**PS2**, **CS2**); (c) films prepared by bulk reaction of formylated polysulfone and chitosan, *via* imine (**PS-CS-I**, **CS-PS-I**) or amine bonds (**PS-CS-R**, **CS-PS-R**); (d)–(i) representative sorption desorption curves of understudied samples.

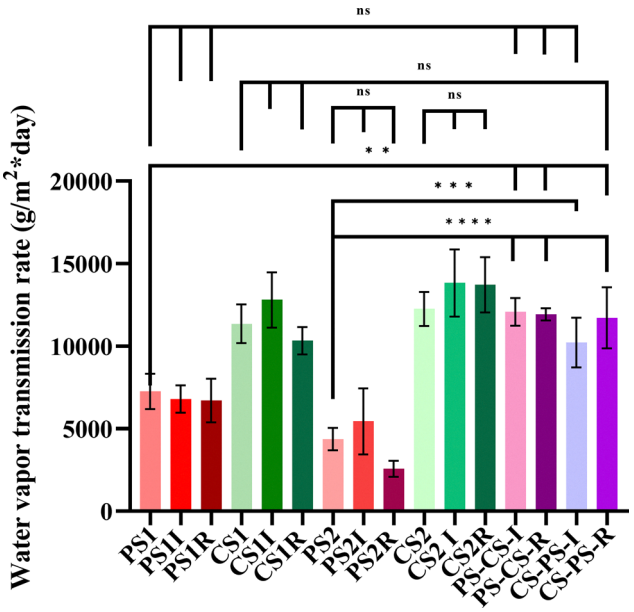

Fig. 11 Average water vapor transmission rate of the investigated materials.

chitosan, thus making the penetration of water vapor more difficult. This can be attributed to the surface modification of the films with chitosan due to the affinity of this polymer for water molecules, which in this way leads to the swelling of the material surface and the creation of a barrier against water penetration through the membrane pores. Also, from the SEM micrographs (Fig. 8) it can be seen that by attaching the chitosan to the surface of formylated polysulfone films, the structure of these membranes becomes more compact.

It should be noted that samples **PS-CS-I**, **PS-CS-R**, **CS-PS-I** and **CS-PS-R** show a high-water vapor transmission performance, higher than that of pure chitosan films or formylated polysulfone, thus showing that the bulk synthesis of chitosan-*g*-polysulfone facilitates the obtaining of films with improved moisture transport, as a result of the intimate dispersion of chitosan and polysulfone macromolecular chains in the polymer matrix (Fig. 11).

3.4. Biologic properties

Enzymatic degradation. While polysulfone is well known for its lack of biodegradability, chitosan stands out for this characteristic. Starting from these premises, it is interesting to see how their combination influences this crucial feature for bioapplications. In this sense, the biodegradation was investigated in wet environments containing lysozyme, an enzyme found in biological fluids, capable of cleaving the β-(1 → 4) glycosidic bonds between D-glucosamine and *N*-acetyl D-glucosamine units in the chitosan structure.[63] As expected, the highest mass loss (up to 46%) was recorded in the case of unmodified chitosan films and xerogels, attributed to the enzymatic degradation and also to chitosan solubilization (Fig. 12).[78]

By grafting polysulfone onto the surface of chitosan materials, the degradation process was significantly hindered, reaching a mass loss percentage lower than 10% after prolonged exposure (21 days) of the materials to the action of lysozyme. This behaviour can be explained by the fact that the hydrophobic layer of polysulfone onto the surface of chitosan materials prevents the penetration of lysozyme into the structure of the material, and implicitly the cleavage of glycosidic bonds in the structure of chitosan. In the case of materials obtained by the bulk condensation, the percentage of mass loss was higher, with values close to those of chitosan materials.[41,59,79] This fact can be explained by the porous nature of the materials which favoured the access of the enzyme to the chitosan domains. The determination of the mass loss rate per day showed that the materials obtained by binding the two polymers *via* bulk reaction exhibit the fastest degradation rate, compared to the surface-functionalized materials, recording a degradation rate of 0.062 ± 0.02 mg per day

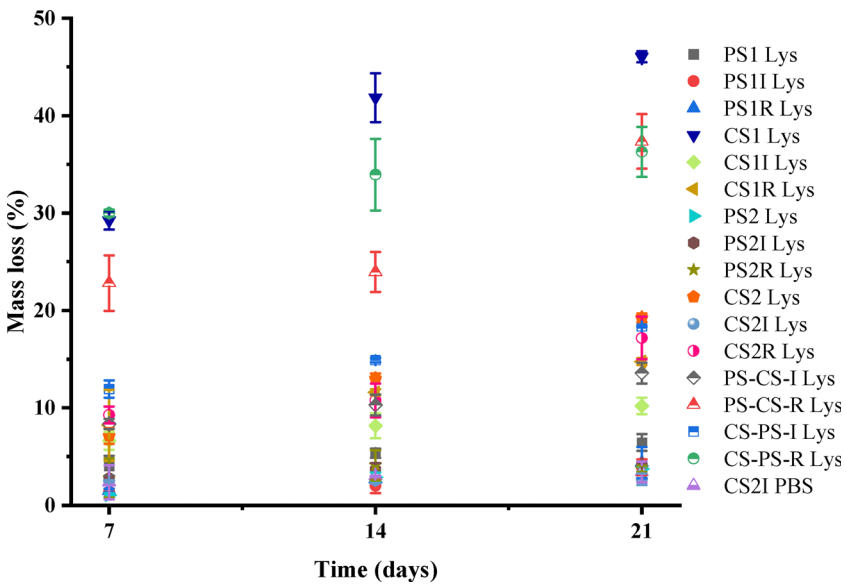

Fig. 12 Graphical representation of the biodegradation kinetics in the presence of lysozyme of the investigated materials.

compared to 0.009 ± 0.0008 mg per day. This is somehow expected, given the known susceptibility of chitosan to enzymatic degradation and its large exposure to the surface biomaterials obtained by bulk synthesis, favoring the degradation. Moreover, as degradation progresses, the emergence of erosion and structural defects further facilitates enzymatic access to the chitosan component. However, estimating the complete degradation timeline of these materials presents a series of difficulties, considering the non-degradable nature of polysulfone.[79]

Antioxidant activity. Chitosan exhibits hydroxyl and amino groups in its structure which can react with free radicals, providing its antioxidant activity.[80] Moreover, several studies have indicated that imine derivatives with hydroxyl groups may exhibit enhanced antioxidant activity due to a synergistic effect between the two functional groups.[81–83] Based on these considerations, the radical scavenging activity of the studied materials was investigated using the DPPH method and the results are presented in Fig. 13. The data recorded indicate that most of the samples show a slight antioxidant activity, which may be influenced by the method of obtaining the material or by its chemical structure. Therefore, the best antioxidant activity was observed in the case of the iminated samples **CS-PS-I**, **PS-CS-I** and **CS2I**, whose performance can be explained by the high amount of chitosan with antioxidant ability, as well as by the improved swelling ability, favouring the access of the radical species to the radical scavenging sites, *i.e.* the functional groups –OH, $–NH_2$ and –C═NH–.[84] In addition, the stronger antioxidant activity of the iminated samples can be explained by the reversibility of this linkage in wet media, which makes available both formyl and amine units with antioxidant activity.[85] It can be seen that linking chitosan to polysulfone through imine bonds *via* bulk synthesis significantly improved this property, recording a much higher inhibition percent of free radicals than in the case of pure polysulfone[86–89] or other polysulfone derivatives,[90] as well as an inhibition higher or similar to that reported for polysulfone hollow fibre membranes functionalized with different concentrations of chitosan diallyl disulfide nanoparticles.[91] These results demonstrate that functionalizing polysulfone with chitosan significantly enhances its antioxidant properties. The synthesis routes developed in this study represent an initial step towards creating materials with a high capacity for inhibiting reactive oxygen species, an essential property for a wide range of biomedical applications, particularly where oxidative stress is a concern, such as drug delivery systems,[92] wound dressings,[93] implants and scaffolds.[94]

Antimicrobial activity. The antimicrobial activity of the sample surfaces was investigated against two bacterial strains, *Staphylococcus aureus* and *Escherichia coli*, using a modified Japanese industrial standard for surfaces. As can be seen in Fig. 14, the samples presented similar antibacterial activity against the two reference strains. As a general trend, the bulk reaction of the two polymers improved the antimicrobial activity compared to the unmodified polysulfone materials, suggesting that the amount of chitosan present in the material structure is relevant for this property.[95–97] In addition, another factor that influenced the bacteriostatic activity of the investigated materials was their morphology, with lower values of bacterial cell viability being recorded in the case of xerogels based on chitosan and polysulfone and of the films obtained by the bulk reaction of the two polymers, in both cases a higher porosity was observed, leading to a larger contact surface between the microorganism and the material and implicitly to a more efficient inhibition. In the case of *S. aureus*, the highest efficiency was shown by **CS1**, **CS1R** and **CS2R** samples, reducing the bacterial populations to 70%, while in the case of *E. coli*, the **CS2R** sample was the most efficient, reducing the bacterial population to 75%. Starting from the premise that the amount of chitosan and the morphology of the material influence the bacteriostatic activity of the materials and analyzing the cell viability values of the two bacterial strains, we can note that the materials based on chitosan and polysulfone showed a better bacteriostatic activity against the Gram-positive

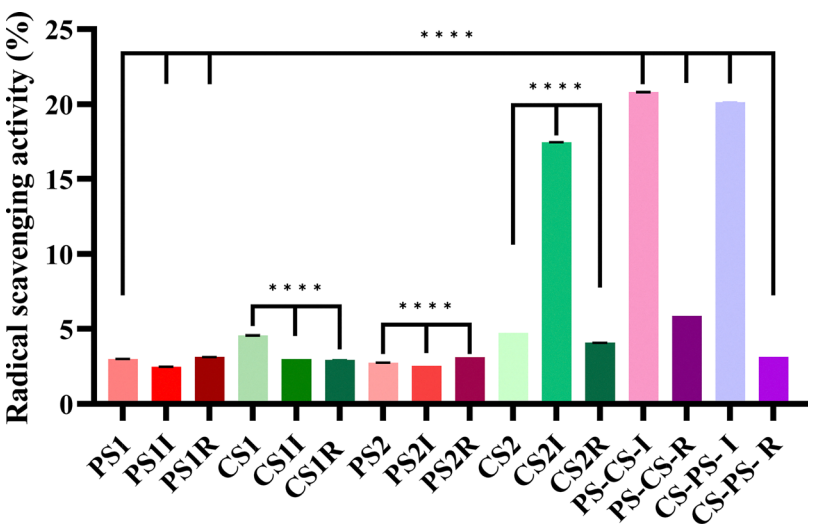

Fig. 13 Antioxidant activity in the solid state of the investigated materials.

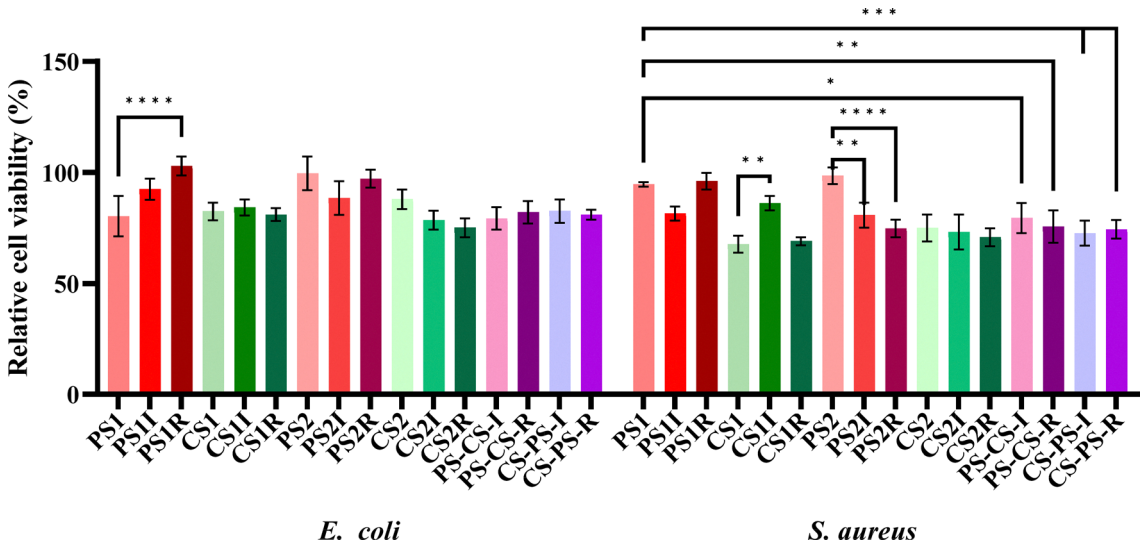

Fig. 14 Antibacterial activity of the samples against *E. coli* and *S. aureus* strains.

bacterium *S. aureus*, a fact also reported in other studies that investigated the antimicrobial activity of chitosan.[98] This aspect can be correlated with the structural differences of the two types of microorganisms, Gram positive *vs.* Gram negative, the lack of the outer membrane in the structure of the *S. aureus* bacteria, which plays a barrier role, facilitates the penetration of chitosan molecules into the structure of the microorganism. In conclusion, we can state that the functionalization of polysulfone with chitosan has a beneficial effect on the capacity to inhibit microorganisms, as has been observed in other studies.[22,99] The results obtained from this study are promising, but further investigations are needed to optimize the composition of the materials so that their bacteriostatic activity becomes stronger.

Conclusions

The study presents a novel strategy for synthesizing chitosan–polysulfone hybrid materials through covalent bonding, achieved either by surface modification or bulk synthesis, *via* imination or amination. Characterization of the resulting materials revealed that covalent integration of chitosan and polysulfone led to semi-crystalline materials with enhanced thermal stability and a porous morphology. Furthermore, the X-ray, DSC and TGA analyses suggested a fine blending of the two polymers *via* interfacial forces. Notably, chitosan incorporation significantly improved hydrophilicity, particularly in bulk-synthesized materials *via* imine bonds, resulting in water uptake of up to 45%, a swelling rate of up to 2 g g^{-1}, water permeability and an antioxidant activity of up to 20%. Additionally, the polysulfone modification with chitosan induced improvements of surface energy, biodegradability in media mimicking the biological fluids and bacteriostatic activity. These findings suggest that imine-bonded chitosan-polysulfone materials represent a promising approach for developing biomaterials with enhanced properties for a broad spectrum of biomedical applications. However, a limitation of this method lies in the challenge of accurately quantifying the extent of covalent bonding between the two polymers using conventional analytical techniques. Addressing this issue should be a priority in future studies to ensure precise characterization and validation of the material's structure.

Conflicts of interest

The authors declare no conflict of interests.

Data availability

The data supporting this article have been included as part of the supplementary information (SI). Supplementary information: Fig. S1. Determination of molecular weight of chitosan by viscosimetry Fig. S2. ^{1}H-NMR spectrum of chitosan recorded in D_2O+HCl Fig. S3. ^{1}H-NMR and ^{13}C-NMR spectra of PSF (a, b) CMPSF (c, d) and FPSF (e, f) with the inset in the ^{1}H-NMR spectra highlighting the overlapping of the signal of CH_3Cl which altered the value of the integral of aromatic protons from 3-C and 3-D Fig. S4. Comparative ^{1}H-NMR spectra of PSF and CMPSF recorded in a) DMSO d_6 and b) $CDCl_3$ Fig. S5. Bidimensional NMR spectra: a) H-H COSY; b) H, C-HMBC; c) H, C-HSQC Fig. S6. SEM-EDAX spectra of the investigated samples Fig. S7. DSC curves of several representative samples during a) heating and b) cooling scan Fig. S8. AFM images of the studied materials Fig. S9. The swelling kinetics of the investigated materials in PBS Fig. S10. Mean static contact angles of the samples with water determined by sessile drop method Fig. S11. Mean static contact angles of the samples with water, ethylene glycol and diiodomethane determined by sessile drop method Fig. S12. Sorption desorption curves of the studied samples Fig. S13. Water vapor transmission rate evolution over 14 days of the investigated materials Table S1. The diffraction angle and corresponding d-spacing of the studied materials Table S2. Parameters of thermal degradation: maxima

degradation temperatures (T_{max}) and corresponding mass loss, as well as the ash residue Table S3. Roughness average (R.a.) values in nm of the investigated samples, measured on surfaces of 5 × 5 μm^2 and 10 × 10 μm^2 Table S4. Surface free energy values (γ_{sv}) and disperse and polar components (γ_{sv}^{d}, γ_{sv}^{p}) for the investigated coatings in mJ m^{-2} Table S5. Surface parameters of the investigated materials based on the sorption/desorption isotherms: sorption capacity (% d.b.), average pore size, specific surface area (m^2 g^{-1}) and the amount of water retained in the monolayer (g/g). See DOI: **https://doi.org/10.1039/d5cp01442e**.

All data will be made available on request.

References

1 T. K. Abbas, K. T. Rashid, S. Al-Saadi, A. A. Alsarayreh, A. Figoli, Q. F. Alsalhy and M. H. Al-Furaiji, Decontamination of Aqueous Nuclear Waste via Pressure-driven Membrane Application – A Short Review, *Eng. Technol. J.*, 2023, **41**, 1152–1174, DOI: **10.30684/ETJ.2023.140193.1454**.

2 M. J. Jaafer, J. A. Al-Najar and Q. F. Alsalhy, Poly(phenyl sulfone) hollow fiber forward osmosis membrane for saline water desalination, *Chem. Eng. Process.*, 2020, **157**, 108119, DOI: **10.1016/J.CEP.2020.108119**.

3 L. R. Sahu, D. Yadav, D. Borah, A. Gogoi, S. Goswami, G. Hazarika, S. Karki, M. Borpatra Gohain, S. V. Sawake, S. V. Jadhav, S. Chatterjee and P. G. Ingole, Polymeric Membranes for Liquid Separation: Innovations in Materials, Fabrication, and Industrial Applications, *Polymers*, 2024, **16**, 3240, DOI: **10.3390/POLYM16233240**.

4 W. K. Al-Musawy, B. M. Ibraheem, T. M. Darwesh, M. H. Al-Furaiji, M. Awad and Q. F. Alsalhy, Synthesis and performance of polysulfone-chitosan ultrafiltration membranes for humic acid removal, *Desalin. Water Treat.*, 2025, **321**, 100939, DOI: **10.1016/J.DWT.2024.100939**.

5 M. Nur-E-Alam, S. A. Deowan, E. Hossain, K. S. Hossain, M. Y. Miah and M. Nurnabi, Fabrication of Polysulfone-Based Microfiltration Membranes and Their Performance Analysis, *Water, Air, Soil Pollut.*, 2024, **235**, 1–17, DOI: **10.1007/S11270-023-06872-X/TABLES/8**.

6 W. K. Al-Musawy, B. M. Ibraheem, T. M. Darwesh, M. H. Al-Furaiji, M. Awad and Q. F. Alsalhy, Synthesis and performance of polysulfone-chitosan ultrafiltration membranes for humic acid removal, *Desalin. Water Treat.*, 2025, **321**, 100939, DOI: **10.1016/J.DWT.2024.100939**.

7 O. Dumbrava, A. Filimon and L. Marin, Tailoring properties and applications of polysulfone membranes by chemical modification: Structure-properties-applications relationship, *Eur. Polym. J.*, 2023, **196**, 112316, DOI: **10.1016/j.eurpolymj.2023.112316**.

8 R. Kumar, A. M. Isloor, A. F. Ismail, S. A. Rashid and T. Matsuura, Polysulfone–Chitosan blend ultrafiltration membranes: preparation, characterization, permeation and antifouling properties, *RSC Adv.*, 2013, **3**, 7855–7861, DOI: **10.1039/C3RA00070B**.

9 M. Z. Zailani, A. F. Ismail, P. S. Goh, S. H. S. Abdul Kadir, M. H. D. Othman, H. Hasbullah, M. S. Abdullah, B. C. Ng, F. Kamal and R. Mustafar, Immobilizing chitosan nanoparticles in polysulfone ultrafiltration hollow fibre membranes for improving uremic toxins removal, *J. Environ. Chem. Eng.*, 2021, **9**, 106878, DOI: **10.1016/J.JECE.2021.106878**.

10 S. Saedi, S. S. Madaeni, A. Arabi Shamsabadi and F. Mottaghi, The effect of surfactants on the structure and performance of PES membrane for separation of carbon dioxide from methane, *Sep. Purif. Technol.*, 2012, **99**, 104–119, DOI: **10.1016/J.SEPPUR.2012.08.028**.

11 C. Tran, N. Hallahan, E. Kosobrodova, J. Tong, P. Thorn and M. Bilek, Plasma Surface Engineering to Biofunctionalise Polymers for β-Cell Adhesion, *Coatings*, 2021, **11**, 1085, DOI: **10.3390/COATINGS11091085**.

12 S. Al Aani, C. J. Wright and N. Hilal, Investigation of UF membranes fouling and potentials as pre-treatment step in desalination and surface water applications, *Desalination*, 2018, **432**, 115–127, DOI: **10.1016/J.DESAL.2018.01.017**.

13 B. M. Ibraheem, S. Al Aani, A. A. Alsarayreh, Q. F. Alsalhy and I. K. Salih, Forward Osmosis Membrane: Review of Fabrication, Modification, Challenges and Potential, *Membranes*, 2023, **13**, 379, DOI: **10.3390/MEMBRANES13040379**.

14 A. V. Bildyukevich, T. V. Plisko, Y. A. Isaichykova and A. A. Ovcharova, Preparation of High-Flux Ultrafiltration Polyphenylsulfone Membranes, *Pet. Chem.*, 2018, **58**, 747–759, DOI: **10.1134/S0965544118090050**.

15 H. Basri, A. F. Ismail and M. Aziz, Polyethersulfone (PES)–silver composite UF membrane: Effect of silver loading and PVP molecular weight on membrane morphology and antibacterial activity, *Desalination*, 2011, **273**, 72–80, DOI: **10.1016/J.DESAL.2010.11.010**.

16 T. V. Plisko, A. V. Bildyukevich, Y. A. Karslyan, A. A. Ovcharova and V. V. Volkov, Development of high flux ultrafiltration polyphenylsulfone membranes applying the systems with upper and lower critical solution temperatures: Effect of polyethylene glycol molecular weight and coagulation bath temperature, *J. Membr. Sci.*, 2018, **565**, 266–280, DOI: **10.1016/J.MEMSCI.2018.08.038**.

17 H. J. Song, Y. J. Jo, S. Y. Kim, J. Lee and C. K. Kim, Characteristics of ultrafiltration membranes fabricated from polysulfone and polymer-grafted silica nanoparticles: Effects of the particle size and grafted polymer on the membrane performance, *J. Membr. Sci.*, 2014, **466**, 173–182, DOI: **10.1016/J.MEMSCI.2014.04.053**.

18 M. Gogoi, A. Borah, R. Goswami, H. Sarmah, A. R. Borah, B. K. Saikia and S. Hazarika, Functionalized carbon nanotube-quantum dot thin film nanocomposite membrane for separation of β-substituted-α-amino acid enantiomers, *React. Funct. Polym.*, 2024, **205**, 106079, DOI: **10.1016/j.reactfunctpolym.2024.106079**.

19 J. Wang, Y. Liu, T. Liu, X. Xu and Y. Hu, Improving the perm-selectivity and anti-fouling property of UF membrane through the micro-phase separation of PSf-*b*-PEG block copolymers, *J. Membr. Sci.*, 2020, **599**, 117851, DOI: **10.1016/J.MEMSCI.2020.117851**.

20 N. Shahkaramipour, S. N. Ramanan, D. Fister, E. Park, S. R. Venna, H. Sun, C. Cheng and H. Lin, Facile Grafting of Zwitterions onto the Membrane Surface to Enhance Antifouling Properties for Wastewater Reuse, *Ind. Eng. Chem. Res.*, 2017, **56**, 9202–9212, DOI: 10.1021/ACS.IECR.7B02378/SUPPL_FILE/IE7B02378_SI_001.PDF.

21 D. Ma, Z. Wang, T. Liu, Y. Hu and Y. Wang, Spray coating of polysulfone/poly(ethylene glycol) block polymer on macroporous substrates followed by selective swelling for composite ultrafiltration membranes, *Chin. J. Chem. Eng.*, 2021, **29**, 85–91, DOI: 10.1016/J.CJCHE.2020.05.002.

22 T. M. Liu, J. J. Xu and Y. R. Qiu, A novel kind of polysulfone material with excellent biocompatibility modified by the sulfonated hydroxypropyl chitosan, *Mater. Sci. Eng., C*, 2017, **79**, 570–580, DOI: 10.1016/J.MSEC.2017.05.103.

23 M. S. Sangeetha, A. Kandaswamy and A. Vijayalakshmi, Preparation and Characterisation of Flat Sheet Micro/Nanoporous Membranes Using Polysulfone Blend With PVP/PEG and Chitosan/Chitosan Nanoparticles for Biomedical Applications, *J. Optoelectron. Biomed. Mater.*, 2016, **8**(2), 81–87.

24 Y. L. Liu, C. H. Yu, L. C. Ma, G. C. Lin, H. A. Tsai and J. Y. Lai, The effects of surface modifications on preparation and pervaporation dehydration performance of chitosan/polysulfone composite hollow-fiber membranes, *J. Membr. Sci.*, 2008, **311**, 243–250, DOI: 10.1016/J.MEMSCI.2007.12.040.

25 A. T. Yasir, A. Benamor, A. H. Hawari and E. Mahmoudi, Graphene oxide/chitosan doped polysulfone membrane for the treatment of industrial wastewater, *Emergent Mater.*, 2023, **6**, 899–910, DOI: 10.1007/s42247-023-00504-0.

26 M. Z. Zailani, A. F. Ismail, P. S. Goh, S. H. S. Abdul Kadir, M. H. D. Othman, H. Hasbullah, M. S. Abdullah, B. C. Ng, F. Kamal and R. Mustafar, Immobilizing chitosan nanoparticles in polysulfone ultrafiltration hollow fibre membranes for improving uremic toxins removal, *J. Environ. Chem. Eng.*, 2021, **9**, 106878, DOI: 10.1016/j.jece.2021.106878.

27 R. Y. M. Huang, R. Pal and G. Y. Moon, Crosslinked chitosan composite membrane for the pervaporation dehydration of alcohol mixtures and enhancement of structural stability of chitosan/polysulfone composite membranes, *J. Membr. Sci.*, 1999, **160**, 17–30, DOI: 10.1016/S0376-7388(99)00074-5.

28 T.-M. Liu, J.-J. Xu and Y.-R. Qiu, A novel kind of polysulfone material with excellent biocompatibility modified by the sulfonated hydroxypropyl chitosan, *Mater. Sci. Eng., C*, 2017, **79**, 570–580, DOI: 10.1016/j.msec.2017.05.103.

29 K. Balakrishna Prabhu, M. B. Saidutta, A. M. Isloor and R. Hebbar, Improvement in performance of polysulfone membranes through the incorporation of chitosan-(3-phenyl-1h-pyrazole-4-carbaldehyde), *Cogent Eng.*, 2017, **4**, 1403005, DOI: 10.1080/23311916.2017.1403005.

30 V. Cozan and E. Avram, Side chain thermotropic liquid crystalline polysulfone obtained from polysulfone udel by chemical modification, *Eur. Polym. J.*, 2003, **39**, 107–114, DOI: 10.1016/S0014-3057(02)00181-7.

31 E. S. Dragan, M. Cazacu and A. Nistor, Ionic organic/inorganic materials. III. stimuli responsive hybrid hydrogels based on oligo(N,N-dimethylaminoethylmethacrylate) and chloroalkyl- functionalized siloxanes, *J. Polym. Sci., Part A:Polym. Chem.*, 2009, **47**, 6801–6813, DOI: 10.1002/POLA.23720;PAGE:STRING:ARTICLE/CHAPTER.

32 R. Mustapha, A. Zoughaib, N. Ghaddar and K. Ghali, Modified upright cup method for testing water vapor permeability in porous membranes, *Energy*, 2020, **195**, 117057, DOI: 10.1016/J.ENERGY.2020.117057.

33 Y. Ren, L. Huang, Y. Wang, L. Mei, R. Fan, M. He, C. Wang, A. Tong, H. Chen and G. Guo, Stereocomplexed electrospun nanofibers containing poly (lactic acid) modified quaternized chitosan for wound healing, *Carbohydr. Polym.*, 2020, **247**, 116754, DOI: 10.1016/J.CARBPOL.2020.116754.

34 Y. Ando, H. Miyamoto, I. Noda, F. Miyaji, T. Shimazaki, Y. Yonekura, M. Miyazaki, M. Mawatari and T. Hotokebuchi, Japanese Industrial Standard Antimicrobial products-Test for antimicrobial activity and efficacy, JIS Z 2801:2000, 2010, pp. 15–19, DOI: 10.4265/BIO.15.15.

35 A. X. de Souza, P. D. Frighetto, G. Badagnani de Carvalho, H. de Castro Degiovani, M. Firmino de Oliveira, C. R. Neri, V. Palaretti, A. M. de Faria, D. Pasquini and L. C. de Morais, Polysulfone with Different Degrees of Sulfonation: Simple Method with Acetyl Sulfate, *Orbital:Electron. J. Chem.*, 2024, **16**, 41–49, DOI: 10.17807/ORBITAL.V15I5.19865.

36 H. Cong, T. Yamato and Z. Tao, Chemo-selective oxidation of hydroxybenzyl alcohols with IBX in the presence of hemicucurbit[6]uril, *New J. Chem.*, 2013, **37**, 3778–3783, DOI: 10.1039/C3NJ00660C.

37 E. Kleinpeter, Quantification and Visualization of the Anisotropy Effect in NMR Spectroscopy by Through-Space NMR Shieldings, *Annu. Rep. NMR Spectrosc.*, 2014, **82**, 115–166, DOI: 10.1016/B978-0-12-800184-4.00003-5.

38 D. Sajan, Y. Erdogdu, T. Kuruvilla and I. H. Joe, Vibrational spectra and first-order molecular hyperpolarizabilities of p-hydroxybenzaldehyde dimer, *J. Mol. Struct.*, 2010, **983**, 12–21, DOI: 10.1016/J.MOLSTRUC.2010.08.003.

39 S. Hallmann, M. J. Fink and B. S. Mitchell, Williamson ether synthesis: an efficient one-step route for surface modifications of silicon nanoparticles, *J. Exp. Nanosci.*, 2015, **10**, 588–598, DOI: 10.1080/17458080.2013.848299.

40 L. Marin, V. Cozan and M. Bruma, Comparative study of new thermotropic polyazomethines, *Polym. Adv. Technol.*, 2006, **17**, 664–672, DOI: 10.1002/PAT.767;JOURNAL:JOURNAL:10991581;WGROUP:STRING:PUBLICATION.

41 M. M. Iftime, I. Rosca, A. I. Sandu and L. Marin, Chitosan crosslinking with a vanillin isomer toward self-healing hydrogels with antifungal activity, *Int. J. Biol. Macromol.*, 2022, **205**, 574–586, DOI: 10.1016/J.IJBIOMAC.2022.02.077.

42 S. Cibotaru, D. Ailincai, B. I. Andreica, X. Cheng and L. Marin, TEGylated Phenothiazine-Imine-Chitosan Materials as a Promising Framework for Mercury Recovery, *Gels*, 2022, **8**, 692, DOI: 10.3390/GELS8110692.

43 V. Deimede, G. A. Voyiatzis, J. K. Kallitsis, L. Qingfeng and N. J. Bjerrum, Miscibility Behavior of Polybenzimidazole/Sulfonated Polysulfone Blends for Use in Fuel Cell

Applications, *Macromolecules*, 2000, **33**, 7609–7617, DOI: 10.1021/MA000165S.

44 S. Dineshkumar, A. Muthusamy, P. Chitra and S. Anand, Synthesis, characterization, optical and electrical properties of thermally stable polyazomethines derived from 4,4′-oxydianiline, *J. Adhes. Sci. Technol.*, 2015, **29**, 2605–2621, DOI: 10.1080/01694243.2015.1079455.

45 L. Marin, E. Perju and M. D. Damaceanu, Designing thermotropic liquid crystalline polyazomethines based on fluorene and/or oxadiazole chromophores, *Eur. Polym. J.*, 2011, **47**, 1284–1299, DOI: 10.1016/J.EURPOLYMJ.2011.03.004.

46 Y. Xue, J. Tian, W. Tian, K. Zhang, J. Xuan and X. Zhang, Spiropyran based recognitions of amines: UV–Vis spectra and mechanisms, *Spectrochim. Acta, Part A*, 2021, **250**, 119385, DOI: 10.1016/J.SAA.2020.119385.

47 J. Kumirska, M. Czerwicka, Z. Kaczyński, A. Bychowska, K. Brzozowski, J. Thöming and P. Stepnowski, Application of Spectroscopic Methods for Structural Analysis of Chitin and Chitosan, *Mar. Drugs*, 2010, **8**, 1567–1636, DOI: 10.3390/MD8051567.

48 L. Marin, D. Ailincai, M. Mares, E. Paslaru, M. Cristea, V. Nica and B. C. Simionescu, Imino-chitosan biopolymeric films. Obtaining, self-assembling, surface and antimicrobial properties, *Carbohydr. Polym.*, 2015, **117**, 762–770, DOI: 10.1016/J.CARBPOL.2014.10.050.

49 N. Mys, R. Van De Sande, A. Verberckmoes and L. Cardon, Processing of Polysulfone to Free Flowing Powder by Mechanical Milling and Spray Drying Techniques for Use in Selective Laser Sintering, *Polymers*, 2016, **8**, 150, DOI: 10.3390/POLYM8040150.

50 S. S. Silva, S. M. C. Menezes and R. B. Garcia, Synthesis and characterization of polyurethane-g-chitosan, *Eur. Polym. J.*, 2003, **39**, 1515–1519, DOI: 10.1016/S0014-3057(03)00013-2.

51 L. Balau, G. Lisa, M. I. Popa, V. Tura and V. Melnig, Physico-chemical properties of Chitosan films, *Cent. Eur. J. Chem.*, 2004, **2**, 638–647, DOI: 10.2478/BF02482727/MACHINEREADABLECITATION/RIS.

52 G. Lisa, E. Avram, G. Paduraru, M. Irimia, N. Hurduc and N. Aelenei, Thermal behaviour of polystyrene, polysulfone and their substituted derivatives, *Polym. Degrad. Stab.*, 2003, **82**, 73–79, DOI: 10.1016/S0141-3910(03)00164-2.

53 A. Blumstein, Polymerization of adsorbed monolayers. II. Thermal degradation of the inserted polymer, *J. Polym. Sci. A*, 1965, **3**, 2665–2672, DOI: 10.1002/POL.1965.100030721.

54 Y. Chen, X. Wu, M. Li, L. Qian and H. Zhou, Mechanically Robust and Flame-Retardant Polylactide Composites Based on In Situ Formation of Crosslinked Network Structure by DCP and TAIC, *Polymers*, 2022, **14**, 308, DOI: 10.3390/POLYM14020308.

55 M. Nisar, L. M. Dos Santos, J. Geshev, M. I. Qadir, S. Khan, G. J. M. Fechine, G. Machado and S. Einloft, Nanoarchitectured composite of polysulfone and carbon-based fillers bearing magnetically stimulable function for efficient CO2 capture, *J. Sci.:Adv. Mater. Devices*, 2024, **9**, 100701, DOI: 10.1016/J.JSAMD.2024.100701.

56 S. Kluge, K. Hartenauer and M. Tutuș, Morphology Behavior of Polysulfone Membranes Made from Sustainable Solvents, *Gases*, 2024, **4**, 133–152, DOI: 10.3390/gases4030008.

57 Y. Feng, H. Gao, D. Wu, Y. Weng, Z. Wang, S. Yu and Z. Wang, Biomimetic Lamellar Chitosan Scaffold for Soft Gingival Tissue Regeneration, *Adv. Funct. Mater.*, 2021, **31**(43), 2105348, DOI: 10.1002/adfm.202105348.

58 C. Chartier, S. Buwalda, H. Van Den Berghe, B. Nottelet and T. Budtova, Tuning the properties of porous chitosan: Aerogels and cryogels, *Int. J. Biol. Macromol.*, 2022, **202**, 215–223, DOI: 10.1016/j.ijbiomac.2022.01.042.

59 R. Lungu, A. Anisiei, I. Rosca, A. I. Sandu, D. Ailincai and L. Marin, Double functionalization of chitosan based nanofibers towards biomaterials for wound healing, *React. Funct. Polym.*, 2021, **167**, 105028, DOI: 10.1016/J.REACTFUNCTPOLYM.2021.105028.

60 N. L. Thomas and A. H. Windle, A theory of case II diffusion, *Polymer*, 1982, **23**, 529–542, DOI: 10.1016/0032-3861(82)90093-3.

61 D. Baskar and T. S. Sampath Kumar, Effect of deacetylation time on the preparation, properties and swelling behavior of chitosan films, *Carbohydr. Polym.*, 2009, **78**, 767–772, DOI: 10.1016/J.CARBPOL.2009.06.013.

62 F. Von Burkersroda, L. Schedl and A. Göpferich, Why degradable polymers undergo surface erosion or bulk erosion, *Biomaterials*, 2002, **23**, 4221–4231, DOI: 10.1016/S0142-9612(02)00170-9.

63 D. Ren, H. Yi, W. Wang and X. Ma, The enzymatic degradation and swelling properties of chitosan matrices with different degrees of N-acetylation, *Carbohydr. Res.*, 2005, **340**, 2403–2410, DOI: 10.1016/J.CARRES.2005.07.022.

64 B. Li, J. Wang, Q. Gui and H. Yang, Drug-loaded chitosan film prepared via facile solution casting and air-drying of plain water-based chitosan solution for ocular drug delivery, *Bioact. Mater.*, 2020, **5**, 577–583, DOI: 10.1016/J.BIOACTMAT.2020.04.013.

65 T. Ehrenfreund-Kleinman, Z. Gazit, D. Gazit, T. Azzam, J. Golenser and A. J. Domb, Synthesis and biodegradation of arabinogalactan sponges prepared by reductive amination, *Biomaterials*, 2002, **23**, 4621–4631, DOI: 10.1016/S0142-9612(02)00209-0.

66 D. Ailincai, D. Pamfil and L. Marin, Multiple bio-responsive polymer dispersed liquid crystal composites for sensing applications, *J. Mol. Liq.*, 2018, **272**, 572–582, DOI: 10.1016/J.MOLLIQ.2018.09.125.

67 Y. Ikada, Surface modification of polymers for medical applications, *Biomaterials*, 1994, **15**, 725–736, DOI: 10.1016/0142-9612(94)90025-6.

68 D. Ailincai and L. Marin, Eco-friendly PDLC composites based on chitosan and cholesteryl acetate, *J. Mol. Liq.*, 2021, **321**, 114466, DOI: 10.1016/J.MOLLIQ.2020.114466.

69 D. Pathote, P. Kumari, V. Singh, D. Jaiswal, R. K. Gautam and C. K. Behera, Biocompatibility evaluation, wettability, and scratch behavior of Ta-coated 316L stainless steel by DC magnetron sputtering for the orthopedic applications, *Surf. Coat. Technol.*, 2023, **459**, 129392, DOI: 10.1016/J.SURFCOAT.2023.129392.

70 N. J. Hallab, K. J. Bundy, K. O'Connor, R. L. Moses and J. J. Jacobs, Evaluation of metallic and polymeric biomaterial

surface energy and surface roughness characteristics for directed cell adhesion, *Tissue Eng.*, 2001, **7**, 55–70, DOI: 10.1089/107632700300003297;JOURNAL:JOURNAL:TEN;PAGE:STRING:ARTICLE/CHAPTER.

71 K. S. W. Sing and R. T. Williams, Physisorption Hysteresis Loops and the Characterization of Nanoporous Materials, *Adsorpt. Sci. Technol.*, 2004, **22**, 773–782, DOI: 10.1260/0263617053499032.

72 K. S. W. Sing, D. H. Everett, R. A. W. Haul, L. Moscou, R. A. Pierotti, J. Rouquerol and T. Siemieniewska, Reporting Physisorption Data for Gas/Solid Systems with Special Reference to the Determination of Surface Area and Porosity, *Pure Appl. Chem.*, 1985, **57**, 603–619, DOI: 10.1351/PAC198557040603/MACHINEREADABLECITATION/RIS.

73 J. Trifol, D. Plackett, P. Szabo, A. E. Daugaard and M. Giacinti Baschetti, Effect of Crystallinity on Water Vapor Sorption, Diffusion, and Permeation of PLA-Based Nanocomposites, *ACS Omega*, 2020, **5**, 15362–15369, DOI: 10.1021/ACSOMEGA.0C01468/ASSET/IMAGES/MEDIUM/AO0C01468_M002.GIF.

74 A. Bejan, A. Anisiei, B. I. Andreica, I. Rosca and L. Marin, Chitosan nanofibers encapsulating copper oxide nanoparticles: A new approach towards multifunctional ecological membranes with high antimicrobial and antioxidant efficiency, *Int. J. Biol. Macromol.*, 2024, **260**, 129377, DOI: 10.1016/J.IJBIOMAC.2024.129377.

75 J. R. Rodríguez-Núñez, T. J. Madera-Santana, D. I. Sánchez-Machado, J. López-Cervantes and H. Soto Valdez, Chitosan/Hydrophilic Plasticizer-Based Films: Preparation, Physicochemical and Antimicrobial Properties, *J. Polym. Environ.*, 2014, **22**, 41–51, DOI: 10.1007/S10924-013-0621-Z.

76 E. S. Lee, S. K. Hong, Y. S. Kim, J. H. Lee and J. C. Won, Preparation and characteristics of cross-linkable polysulfone having methylene methacrylate side-chain, *J. Appl. Polym. Sci.*, 2008, **109**, 1–8, DOI: 10.1002/APP.27944.

77 S. Noorani, J. Simonsen and S. Atre, Nano-enabled microtechnology: Polysulfone nanocomposites incorporating cellulose nanocrystals, *Cellulose*, 2007, **14**, 577–584, DOI: 10.1007/S10570-007-9119-Y/FIGURES/6.

78 A. Pandit, A. Indurkar, C. Deshpande, R. Jain and P. Dandekar, A systematic review of physical techniques for chitosan degradation, *Carbohydr. Polym. Technol. Appl.*, 2021, **2**, 100033, DOI: 10.1016/j.carpta.2021.100033.

79 M.-M. Iftime, L. Mititelu Tartau and L. Marin, New formulations based on salicyl-imine-chitosan hydrogels for prolonged drug release, *Int. J. Biol. Macromol.*, 2020, **160**, 398–408, DOI: 10.1016/j.ijbiomac.2020.05.207.

80 I. Aranaz, A. R. Alcántara, M. C. Civera, C. Arias, B. Elorza, A. H. Caballero and N. Acosta, Chitosan: An Overview of Its Properties and Applications, *Polymers*, 2021, **13**, 3256, DOI: 10.3390/POLYM13193256.

81 N. R. Rahmawati, Ngadiwiyana, N. B. A. Prasetya, P. R. Sarjono, Y. Andriani and D. F. Syamsumir, Ismiyarto, Synthesis of hydroxylated azomethine compounds and the antioxidant activity, *AIP Conf. Proc.*, 2020, **2237**(1), 020023, DOI: 10.1063/5.0005806/1007483.

82 D. Tomczyk, W. Bukowski, K. Bester, S.-H. Hsiao, H.-Y. Lu, I. Ismiyarto, N. Rizki, N. Ngadiwiyana, P. R. Sarjono and N. B. A. Prasetya, Synthesis of derivatives azomethine compounds bonded to alkoxylated benzene and their antibacterial activity tests, *J. Phys.: Conf. Ser.*, 2020, **1524**, 012090, DOI: 10.1088/1742-6596/1524/1/012090.

83 M. M. Iftime, G. L. Ailiesei, S. Shova, C. Miron, H. Tanaka, M. Hori and L. Marin, New betulin imine derivatives with antioxidant and selective antitumor activity, *New J. Chem.*, 2023, **47**, 16551–16563, DOI: 10.1039/D3NJ02738D.

84 A. Wan, Q. Xu, Y. Sun and H. Li, Antioxidant activity of high molecular weight chitosan and N,O-quaternized chitosans, *J. Agric. Food Chem.*, 2013, **61**, 6921–6928, DOI: 10.1021/JF402242E/ASSET/IMAGES/MEDIUM/JF-2013-02242E_0009.GIF.

85 M. M. Iftime, G. L. Ailiesei and D. Ailincai, Tuning Antioxidant Function through Dynamic Design of Chitosan-Based Hydrogels, *Gels*, 2024, **10**, 655, DOI: 10.3390/GELS10100655/S1.

86 N. Yang, X. Jia, D. Wang, C. Wei, Y. He, L. Chen and Y. Zhao, Silibinin as a natural antioxidant for modifying polysulfone membranes to suppress hemodialysis-induced oxidative stress, *J. Membr. Sci.*, 2019, **574**, 86–99, DOI: 10.1016/J.MEMSCI.2018.12.056.

87 X. Qi, N. Yang, Y. Luo, X. Jia, J. Zhao, X. Feng, L. Chen and Y. Zhao, Resveratrol as a plant type antioxidant modifier for polysulfone membranes to improve hemodialysis-induced oxidative stress, *Mater. Sci. Eng., C*, 2021, **123**, 111953, DOI: 10.1016/J.MSEC.2021.111953.

88 G. Wang, N. Yang, Y. Luo and Y. Zhao, Additive-free preparation of hemodialysis membranes from silibinin-modified polysulfone polymer with enhanced performance in anti-oxidative stress and hemocompatibility, *J. Membr. Sci.*, 2025, **713**, 123345, DOI: 10.1016/j.memsci.2024.123345.

89 P. Wang, N. Yang, Y. Luo, G. Wang, S. Zhou, S. Huang, L. Chen and Y. Zhao, Silymarin modified polysulfone hollow fiber membranes with antioxidant, anti-M1 macrophage polarization and hemocompatibility for blood purification, *J. Biomed. Mater. Res., Part B*, 2023, **111**, 1785–1799, DOI: 10.1002/jbm.b.35285.

90 O. Dumbrava, I. Rosca, D. Ailincai and L. Marin, Quaternized Polysulfones as Matrix for the Development of Broad-Spectrum Antimicrobial Coatings for Medical Devices, *Polymers*, 2025, **17**, 1869, DOI: 10.3390/POLYM17131869/S1.

91 M. Z. Zailani, J. Jaafar, P. S. Goh, S. H. S. A. Kadir, M. H. D. Othman, S. N. A. Ahmad, Y. Raharjo, I. S. Yudaniayanti, D. Santoso and A. F. Ismail, Hemocompatible chitosan nanoparticle diallyl disulfide-modified polysulfone hollow fibre membrane with antithrombotic and antioxidant properties for haemodialysis applications, *Int. J. Biol. Macromol.*, 2025, **305**, 141231, DOI: 10.1016/j.ijbiomac.2025.141231.

92 S. Liu, S. Song, Y. Zhang, L. Yan, Y. Chen, W. Li, B. Jalil, C. Wu, Y. Fu, X. Chen, J. Gu, L. Li, Z. Yin, X. Song, M. Tian and Y. Zou, Delivery of penetration-enhancing antioxidant polyphenol nanoparticles with Codonopsis pilosula polysaccharide microneedles for synergistic treatment of

psoriasis, *Carbohydr. Polym.*, 2025, **363**, 123777, DOI: 10.1016/j.carbpol.2025.123777.

93 X. Liu, Y. Sun, J. Wang, Y. Kang, Z. Wang, W. Cao, J. Ye and C. Gao, A tough, antibacterial and antioxidant hydrogel dressing accelerates wound healing and suppresses hypertrophic scar formation in infected wounds, *Bioact. Mater.*, 2024, **34**, 269–281, DOI: 10.1016/J.BIOACTMAT.2023.12.019.

94 Y. Zhu, D. Zhou, X. Zan, Q. Ye and S. Sheng, Engineering the surfaces of orthopedic implants with osteogenesis and antioxidants to enhance bone formation in vitro and in vivo, *Colloids Surf., B*, 2022, **212**, 112319, DOI: 10.1016/J.COLSURFB.2022.112319.

95 S. Zivanovic, J. Li, P. M. Davidson and K. Kit, Physical, Mechanical, and Antibacterial Properties of Chitosan/PEO Blend Films, *Biomacromolecules*, 2007, **8**, 1505–1510, DOI: 10.1021/bm061140p.

96 N. Ignjatović, V. Wu, Z. Ajduković, T. Mihajilov-Krstev, V. Uskoković and D. Uskoković, Chitosan-PLGA polymer blends as coatings for hydroxyapatite nanoparticles and their effect on antimicrobial properties, osteoconductivity and regeneration of osseous tissues, *Mater. Sci. Eng., C*, 2016, **60**, 357–364, DOI: 10.1016/j.msec.2015.11.061.

97 P. Fernandez-Saiz, J. M. Lagaron, P. Hernandez-Muñoz and M. J. Ocio, Characterization of antimicrobial properties on the growth of S. aureus of novel renewable blends of gliadins and chitosan of interest in food packaging and coating applications, *Int. J. Food Microbiol.*, 2008, **124**, 13–20, DOI: 10.1016/j.ijfoodmicro.2007.12.019.

98 Y. Tao, L.-H. Qian and J. Xie, Effect of chitosan on membrane permeability and cell morphology of Pseudomonas aeruginosa and Staphyloccocus aureus, *Carbohydr. Polym.*, 2011, **86**, 969–974, DOI: 10.1016/j.carbpol.2011.05.054.

99 M. M. Tu, J. J. Xu and Y. R. Qiu, Surface hemocompatible modification of polysulfone membrane via covalently grafting acrylic acid and sulfonated hydroxypropyl chitosan, *RSC Adv.*, 2019, **9**, 6254–6266, DOI: 10.1039/C8RA10573A.